MICROCOPY RESOLUTION TEST CHART

NATIONAL BUREAU OF STANDARDS-1963-A

AFFDL-TR-79-3030

FORMULATION OF THE THREE-DIMENSIONAL TRANSONIC UNSTEADY AERODYNAMIC PROBLEM

H. Yoshihara

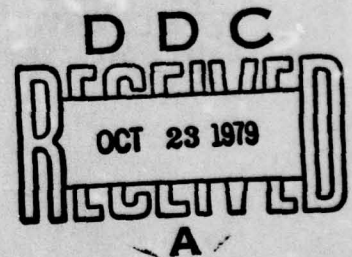BOEING MILITARY AIRPLANE DEVELOPMENT
The Boeing Company
P. O. Box 3999
Seattle, Washington   98124

February 1979

DDC
RECEIVED
OCT 23 1979
A

AIR FORCE FLIGHT DYNAMICS LABORATORY
AIR FORCE WRIGHT AERONAUTICAL LABORATORIES
AIR FORCE SYSTEMS COMMAND
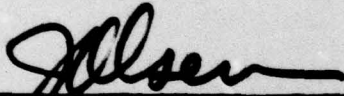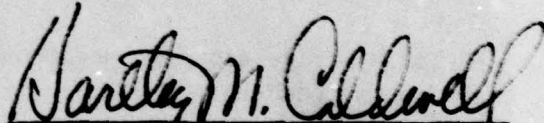WRIGHT-PATTERSON AIR FORCE BASE, OHIO   45433

79 10 23 004

NOTICE

When Government drawings, specifications, or other data are used for any purpose other than in connection with a definitely related Government procurement operation, the United States Government thereby incurs no responsibility nor any obligation whatsoever; and the fact that the government may have formulated, furnished, or in any way supplied the said drawings, specifications, or other data, is not to be regarded by implication or otherwise as in any manner licensing the holder or any other person or corporation, or conveying any rights or permission to manufacture, use, or sell any patented invention that may in any way be related thereto.

This report has been reviewed by the Information Office (OI) and is releasable to the general public, including foreign nations.

This technical report has been reviewed and is approved for publication.
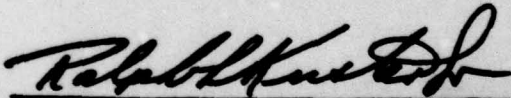
James G. Olsen, Principal Scientist
Analysis & Optimization Branch

HARTLEY M. CALDWELL, III, Capt, USAF
Actg Ch, Analysis & Optimization Branch

FOR THE COMMANDER

Ralph L. Kuster, Jr., Col. USAF
Chief, Structures and Dynamics Div.

"If your address has changed, if you wish to be removed from our mailing list, or if the addressee is no longer employed by your organization, please notify FBR, W-PAFB, OH 45433 to help us maintain a current mailing list".

Copies of this report should not be returned unless return is required by security considerations, contractual obligations, or notice on a specific document.

REPORT DOCUMENTATION PAGE	READ INSTRUCTIONS BEFORE COMPLETING FORM

1. REPORT NUMBER	2. GOVT ACCESSION NO.	3. RECIPIENT'S CATALOG NUMBER
AFFDL-TR-79-3030		

4. TITLE (and Subtitle)	5. TYPE OF REPORT & PERIOD COVERED
FORMULATION OF THE THREE DIMENSIONAL TRANSONIC UNSTEADY AERODYNAMIC PROBLEM	Interim Report 15 May 1978-15 February 1979
	6. PERFORMING ORG. REPORT NUMBER

7. AUTHOR(s)	8. CONTRACT OR GRANT NUMBER(s)
H. Yoshihara	F33615-78-C-3201

9. PERFORMING ORGANIZATION NAME AND ADDRESS	10. PROGRAM ELEMENT, PROJECT, TASK AREA & WORK UNIT NUMBERS
The Boeing Company (BMAD) P.O. Box 3999 Seattle, WA 98124	PE 62201F; WU 24010224

11. CONTROLLING OFFICE NAME AND ADDRESS	12. REPORT DATE
Air Force Flight Dynamics Laboratory (FBR) Air Force Systems Command Wright-Patterson Air Force Base, OH 45433	February 1979
	13. NUMBER OF PAGES
	78

14. MONITORING AGENCY NAME & ADDRESS(if different from Controlling Office)	15. SECURITY CLASS. (of this report)
	Unclassified
	15a. DECLASSIFICATION/DOWNGRADING SCHEDULE

16. DISTRIBUTION STATEMENT (of this Report)

Approved for public release; distribution unlimited

17. DISTRIBUTION STATEMENT (of the abstract entered in Block 20, if different from Report)

18. SUPPLEMENTARY NOTES

19. KEY WORDS (Continue on reverse side if necessary and identify by block number)

Transonic flow	Theoretical
Unsteady flow	Wall interference
Small disturbance	Viscous interactions

20. ABSTRACT (Continue on reverse side if necessary and identify by block number)

Unsteady transonic flow for a swept wing of moderate sweep is formulated in the small disturbance limit. Boundary conditions at the wing, the trailing vortex sheet, and the outer computational boundaries are given including the ventilated wall conditions. Shortcomings of the small disturbance hypothesis is reviewed, suggesting means to compensate for them. Viscous interactions are described together with procedures to incorporate their effects.

DD FORM 1473 EDITION OF 1 NOV 65 IS OBSOLETE
1 JAN 73

410258

FOREWORD

This report was prepared by Boeing Military Airplane Development, The Boeing Company, Seattle, Washington, for the Structural Integrity Branch, and the Analysis and Optimization Branch of the Structural Mechanics Division, Air Force Flight Dynamics Laboratory, Wright Aeronautical Laboratories, Wright-Patterson Air Force Base, Ohio. Boeing conducted the work under Contract F33615-78-C-3201, "Transonic Unsteady Aerodynamics for Aeroelastic Applications" under Project 2401, and Task 02. Dr. James Olsen of the Structures and Dynamics Division is the AFFDL Project Engineer.

The Interim Report was prepared during the period May 15, 1978 to February 15, 1979.

The Project Manager for Boeing was Dr. H. Yoshihara and the Principal Investigator was C. J. Borland.

TABLE OF CONTENTS

LIST OF ILLUSTRATIONS

LIST OF SYMBOLS

c	wing mean chord
C_E	entrainment function
C_f	skin friction coefficient
C_P	pressure coefficient
δ	boundary layer thickness
δ^*	displacement thickness
γ	ratio of specific heats
H	form factor (δ^*/θ)
σ	time scaling
K,K'	slotted wall parameters
λ	shock sweep also lag constant (Eq. 29)
M_∞	freestream Mach number
p	static pressure
p_∞	freestream pressure
Φ	velocity potential
φ	perturbation potential
R	perforated wall porosity
R_θ	Reynolds number based upon θ
ρ	density
ρ_∞	freestream density
ρ_e	density at the outer edge of the boundary layer
T	time
t	time (non-dimensional)

LIST OF SYMBOLS (CONCLUDED)

τ_o	characteristic time (C/U_∞)
τ_{max}	maximum shear
τ_w	wall shear
θ	momentum thickness
θ_w	streamline slope near wall
U_∞	freestream velocity
U_e	streamwise velocity at edge of boundary layer
U_s	shock speed
V_e	transverse velocity at edge of boundary layer
X,Y,Z	cartesian coordinates
x,y,z	cartesian coordinates (non-dimensional)
x_{TE}	wing trailing edge abscissa
ξ,η,ζ	sheared coordinates

(other symbols are defined in the Appendix)

SECTION I
SUMMARY

The problem of the unsteady transonic flow for a swept wing of moderate sweep is formulated in the small disturbance limit. The steady terms in the resulting potential equation contain the second order sweep terms developed at NLR (Amsterdam) to capture the important swept shocks. The boundary conditions at the wing, the trailing vortex sheet, and the outer computational boundaries are given. Ventilated wall conditions are reviewed as well as the resonant wall interference effects. The shortcomings of the small disturbance hypothesis is described, suggesting means to compensate for them. Finally the important viscous interactions are described together with procedures to incorporate their effects.

SECTION II
INTRODUCTION

The transonic regime is a potential troublespot for aeroelastic problems of high performance aircraft. This is not surprising because of the well known sensitivity of the flow to small perturbations in the boundary condition at the wing or in the freestream. The consequence of this sensitivity is magnified by the presence of shock waves, the movement of which can cause large changes of the lift and moment on the wing.

Our primary objective in the following will be the formulation of the unsteady transonic initial-boundary value problem in the small disturbance limit applicable for aeroelastic problems of swept wings. An essential requisite here is the derivation of the flow equation in the proper conservation form to capture the important moving shock waves. Such an objective can be carried out in a straightforward manner using the well established results for the steady case. (See References 1 and 2.) A secondary, but still important, objective is to review the important viscous interactions playing an essential role in the positioning and movement of shock waves, and to describe possible means to incorporate their effects in a manner that will ultimately not add significantly to the computer time.

In a formal derivation of the small disturbance problem, a perturbation potential is introduced in both the flow equation and the boundary conditions, and an expansion then carried out. A scaling of the independent and dependent variables and a physically meaningful limiting process are then introduced to seek a nontrivial problem to the lowest order. In the planar steady case, the result was the familiar problem embodying the classical transonic similarity. The same similarity limiting procedure applied to the three dimensional (3D) case, yielded a 3D flow equation containing only the Φ_{yy} term to represent the spanwise

effects (Reference 3). A subsequent examination of the shock jump condition implied by this equation showed that only shocks essentially normal to the freestream were properly captured, precluding the proper capture of swept shocks (Reference 1). By adding two higher order "sweep" terms, Bailey, Ballhaus, and Lomax (Reference 1) showed that the proper shock condition was obtained for swept shocks arising in the case of a constant chord yawed wing of infinite aspect ratio. Later van der Vooren, Slooff, Huizing, and van Essen (Reference 2) by a different expansion found that by adding the same sweep terms but with different (constant) coefficients, in addition, the more highly swept forward shock typically appearing in swept wings was also correctly captured.

The above higher order potential equations derived in References 1 and 2 for the steady 3D case cannot be formally derived in a consistent way by a similarity limiting process. Thus in the derivation of the unsteady 3D equation applicable for swept wings, we shall similarly dispense with limiting processes and simply add the necessary second order terms to capture the important swept shocks.

In the following, after deriving the proper flow equation, we shall describe the boundary condition on the wing, the contact conditions on the trailing vortex sheet, and the outer far-field conditions. Also the ventilated wall condition will be reviewed. Limitations of the resulting inviscid small disturbance formulation will next be discussed, with suggestions for their compensation. Finally, the dominant viscous interactions will be reviewed, followed by means to incorporate their effects in the computations.

3

SECTION III
FORMULATION OF THE PROBLEM

In the present section we shall formulate the small disturbance problem starting with the exact potential equation. A more general formulation is given in more detail in the Appendix.

1.0 BASIC FLOW EQUATIONS (REFERENCES 4 & 5)

Our starting point is the exact unsteady potential equation given by

$$(\rho)_T + (\rho \Phi_X)_X + (\rho \Phi_Y)_Y + (\rho \Phi_Z)_Z = 0 \tag{1}$$

where

$$\frac{\rho}{\rho_\infty} = 1 - (\gamma - 1) M_\infty^2 \left[U_\infty^{-2} \Phi_T + \frac{1}{2} \left\{ U_\infty^{-2} (\Phi_X^2 + \Phi_Y^2 + \Phi_Z^2) - 1 \right\} \right]^{\frac{1}{\gamma - 1}} \tag{2}$$

Here subscripts denote partial differentiations, and

$\quad \rho \quad$ is the density [slugs/ft3]

$\quad \Phi \quad$ the velocity potential [ft2/sec]

$X, Y, Z \quad$ Cartesian coordinates (X-streamwise; Y-"spanwise") [ft]

$\quad T \quad$ time [sec]

$\quad \gamma \quad$ ratio of specific heats

$\quad U_\infty \quad$ freestream velocity [ft/sec]

$\quad M_\infty \quad$ freestream Mach number, and

$\quad \rho_\infty \quad$ freestream density. [slugs/ft3]

4

Eq. (1) is the mass conservation equation in divergence form, and it is of hyperbolic type independent of the local Mach number.

We next introduce the perturbation potential and simultaneously nondimensionalize the variables as follows:

$$\Phi(X,Y,Z,T) = U_\infty c \left[x + \varphi(x,y,z,t) \right]$$

$$X = cx \qquad Y = cy \qquad Z = cz \qquad (3)$$

$$T = (\sigma c / U_\infty) t$$

where $\quad$ c is the wing reference chord [ft] , and

$\quad\quad\quad$ σ a nondimensional scaling factor on the time.*

The perturbation potential is next introduced into Eqs. (1) and (2), and an expansion carried out retaining only those quadratic terms needed to yield the proper steady shock jump conditions for relevent swept shocks. We obtain,

$$\nabla \cdot \bar{f} = 0$$

where

$$\bar{f} = \bar{h} f_0 + \bar{\imath} f_1 + \bar{\jmath} f_2 + \bar{k} f_3 \qquad (4)$$

$$f_0 = -\sigma (\sigma \varphi_t + \varphi_x)$$

$$f_1 = \left(\frac{1 - M_\infty^2}{M_\infty^2} \right) \varphi_x - \frac{1}{2}(\gamma+1)\left\{ 1 - \left(\frac{\gamma-2}{\gamma+1}\right)(1 - M_\infty^2) \right\} \varphi_x^2 - k \varphi_t - \frac{1}{2}\varphi_y^2$$

$$f_2 = (1 - M_\infty^2 \varphi_x) \varphi_y M_\infty^{-2}$$

$$f_3 = \varphi_z M_\infty^{-2}$$

---

* A scaling σ of the time is introduced here solely to identify limiting cases. For the computer program we will set $\sigma = 1$.

-5-

$\bar{h}, \bar{\imath}, \bar{\jmath}, \bar{k}$ are the unit vectors in the t, x, y and z directions.

Eq. (4) has been expressed in the vector form to facilitate the derivation of the shock jump conditions. It is to be noted that this equation ceases to be valid when the unsteadiness becomes too severe (large σ) as in the case of a "gust" problem modeled by an abrupt increase in angle of attack. Here the neglected time derivatives as the φ_{zt} given in the Appendix will have a significant influence. We shall see later that the small disturbance wing boundary condition will also become invalid for large σ.

2.0 Shock Jump Conditions (Reference 6)

The shock surface will be defined by $s(x,y,z,t) = 0$. The normal vector to this surface will then be given by,

$$\bar{n}_s = (\bar{h} s_t + \bar{\imath} s_x + \bar{\jmath} s_y + \bar{k} s_z)(s_t^2 + s_x^2 + s_y^2 + s_z^2)^{-\frac{1}{2}}$$

On s = 0 we have

$$ds = s_t \, dt + s_x \, dx + s_y \, dy + s_z \, dz = 0 \tag{5}$$

The shock velocity components (U_s, V_s, W_s) are given by

$$U_s = \frac{dx}{dt}\Big|_{s=0} \qquad V_s = \frac{dy}{dt}\Big|_{s=0} \qquad W_s = \frac{dz}{dt}\Big|_{s=0}$$

so that the above equation becomes

$$S_t + U_s S_x + V_s S_y + W_s S_z = 0 . \tag{6}$$

The shock jump conditions are based upon the continuity equation

$$\nabla \cdot \bar{f} = 0$$

6

together with the supplementary differentiability conditions

$$(\varphi_x)_t = (\varphi_t)_x$$

$$(\varphi_y)_t = (\varphi_t)_y$$

$$(\varphi_z)_t = (\varphi_t)_z ,$$

or in "tensor" notation

$$\nabla \cdot \bar{M} = 0$$

where

$$\bar{M} = \bar{h} \begin{Bmatrix} f_o \\ \varphi_x \\ \varphi_y \\ \varphi_z \end{Bmatrix} + \bar{i} \begin{Bmatrix} f_1 \\ -\varphi_t \\ 0 \\ 0 \end{Bmatrix} + \bar{j} \begin{Bmatrix} f_2 \\ 0 \\ -\varphi_t \\ 0 \end{Bmatrix} + \bar{k} \begin{Bmatrix} f_3 \\ 0 \\ 0 \\ -\varphi_t \end{Bmatrix}$$

To derive the shock jump conditions, we first define a control surface formed by the upstream and downstream faces of a shock surface element and introduce Green's formulae equating the volume integral of $\nabla \cdot \bar{M}$ to the surface integral of the flux of $\bar{M}$. We obtain directly

$$[\bar{M}] \cdot \bar{n}_s = 0$$

where $[\bar{M}] = \bar{M}_1 - \bar{M}_2$ the subscripts 1 and 2 denoting respectively the upstream and downstream faces of the shock; that is,

$$[f_o] s_t + [f_1] s_x + [f_2] s_y + [f_3] s_z = 0$$

$$[\varphi_x] s_t + [\varphi_t] s_x \qquad\qquad = 0$$

$$[\varphi_y] s_t \qquad + [\varphi_t] s_y \qquad = 0$$

$$[\varphi_z] s_t \qquad\qquad + [\varphi_t] s_z = 0 \qquad (7)$$

7

Because of the second equation in Eq. (7), we can transfer the φ_t occurring in f_1 in the first equation to the f_0 term. This is usually done, as in LTRAN2 (Reference 31), to simplify the numerical algorithm. Eqs. (6) and (7) then constitute the shock jump conditions.

It will be reassuring to consider next several familiar simplified cases - namely, the one-dimensional normal shock propagating in a uniform steady upstream flow and the steady three-dimensional (3D) swept shock case.

In the case of the unsteady normal shock, Eqs. (6) and (7) simplify to

$$S_t + U_s\, S_x = 0$$

$$-\sigma\left[\sigma\varphi_t + \varphi_x\right]S_t + \left[K\varphi_x - B\varphi_x^2 - \sigma\varphi_t\right]S_x = 0 \qquad K = \frac{1-M_\infty^2}{M_\infty^2}$$

$$\left[\varphi_x\right]S_t - \left[\varphi_t\right]S_x = 0 \qquad B = \tfrac{1}{2}(\gamma+1)\left\{1 - \left(\frac{\gamma-3}{\gamma+1}\right)\left(1-M_\infty^2\right)\right\}$$

Using the first equation in the second and third equations to eliminate the shape derivatives and introducing a galilean transformation $\xi = x - U_s t$ with $\widetilde{\varphi}(\xi) = \varphi(x,t)$ we obtain the jump condition

$$\varphi_{\xi_1} + \varphi_{\xi_2} = \frac{1}{B}\left\{K + \sigma U_s(2-\sigma U_s)\right\}$$

with

$$U_s = -\left(\frac{\varphi_{t_1} - \varphi_{t_2}}{\varphi_{x_1} - \varphi_{x_2}}\right).$$

Consider next the steady 3D case. From Eqs. (5) and (7) we obtain the jump conditions

8

$$\left[\left(\frac{1-M_\infty^2}{M_\infty^2}\right)\varphi_x - \frac{1}{2}(\gamma+1)\left\{1-\left(\frac{\gamma-2}{\gamma+1}\right)(1-M_\infty^2)\right\}\varphi_x^2 - \frac{1}{2}\bar{M}_\infty^2\varphi_y^2\right]S_x + \left[(1-M_\infty^2\varphi_x)\varphi_y\right]S_y + \left[\varphi_z\right]S_z = 0$$

$$(8)$$

$$S_x + S_y\left.\frac{dy}{dx}\right|_{S=0} + S_z\left.\frac{dz}{dx}\right|_{S=0} = 0$$

These steady jump conditions were first derived by van der Vooren, Slooff, Huizing, and van Essen (Reference 2) who showed that the jump condition given above closely approximated the exact oblique shock condition for both the yawed wing shock as well as for the more highly swept (and thereby weaker) forward shock. (See the curves labeled as NLR in Figure 1 from Reference 2).

Bailey, Ballhaus, and Lomax (Reference 1) earlier derived an alternate steady small disturbance equation starting with the exact flow equations in a different form than Eq. (1). In Reference 2 the shock jump conditions implied by the Bailey-Ballhaus equation were also investigated for the yawed and forward shocks. The primary difference with respect to the NLR equation was a less accurate capture of the forward shock. (See curves labeled as NASA in Figure 1.) Note also in Figure 1 the inadequate jump condition for the classical 3D equation with only the φ_{yy} term (curve labeled Guderley-von Karman).

There was, however, considerable difficulty in capturing the weak forward shock in a steady finite difference calculation even using the more exact NLR equation. This was due to the fact that such highly swept shocks acquired a profile spreading over many more mesh points than the three or so mesh points for less swept stronger shocks as a result of the more pronounced diffusive effects. As a result, even using a relatively refined mesh about the forward shock, the capture was still not fully satisfactory as can be seen in Figure 2.

9

On the other hand, there is usually little need to capture the forward shock sharply, since the important primary terminating shock is reasonably well captured even in the presence of a smeared and poorly captured forward shock.[*] This can be seen in Figure 2 for the NLR equation or in Figure 3 for the NASA equation for the same ONERA wing at a smaller angle of attack.

Thus in an unsteady calculation the improved capture of the forward shock probably is not warranted, so that the steady terms from either the NLR or the NASA equation should suffice. But since the NLR equation is no more complex than the NASA equation, we shall adopt the steady terms from the NLR equation. Thus for our unsteady equation, we shall use

$$-\sigma\left(\sigma\varphi_t + 2\varphi_x\right)_t + \left[\left(\frac{1-M_\infty^2}{M_\infty^2}\right)\varphi_x - \frac{1}{2}(\gamma+1)\left\{1-\left(\frac{\gamma-2}{\gamma+1}\right)(1-M_\infty^2)\right\}\varphi_x^2 - \frac{1}{2}\varphi_y^2\right]_x + M_\infty^{-2}\left[(1-M_\infty^2\varphi_x)\varphi_y\right]_y \quad (9)$$

$$+ M_\infty^{-2}(\varphi_z)_z = 0$$

where the φ_t in the second term has been moved to the first term.

It is clearly evident that no stretching of the coordinates can equalize the order of the terms in this equation. More significantly, similarity laws will not formally exist for the unsteady 3D small disturbance flows described by Eq. (9). (See Appendix.)

In the case of the purely subcritical or purely supersonic flow, the higher order terms in the above equation are indeed higher order in the absence of transonic shocks, and one obtains in the limit the classical Prandtl-Glauert or the Ackeret linear equation.

---

[*] Except of course when the forward and rear shocks approach each other.

Finally, in the limit consistent with the small disturbance approximation, the pressure coefficient is given by;

$$C_p = \frac{P - P_\infty}{\frac{1}{2}\rho_\infty U_\infty^2} = -2\left(\varphi_x + \sigma \varphi_t\right)$$

(10)

3.0 COORDINATE SYSTEM

Consider next the choice of the coordinate system to be used for a general swept wing in a finite difference procedure. Here the experience gained in the steady case will be directly relevent. Of particular concern here is to select a coordinate system which will not require an excessive number of mesh planes in the spanwise direction. Thus, for example, if we assume a cartesian system, it is clear that for a swept wing the spanwise row of mesh points cutting across the leading edge or across a shock will encounter severe spanwise flow gradients as in the φ_{xy} and φ_{yy} terms. This then will necessitate a fine spanwise spacing of the mesh points. Thus in the steady case, Bailey and Ballhaus (Reference 7) introduced the shearing transformation given by

$$\xi = \frac{x - x_{LE}(y)}{c(y)}$$

$$\eta = y$$

$$\zeta = z$$

where $x = x_{LE}(y)$ is the equation of the leading edge of the wing, and $c(y)$ is the spanwise chord distribution. The above transformation maps the swept tapered wing in the (x,y,z) space to a rectangular wing in the (ξ, η, ζ) space. In the transformed plane the mesh configuration is now conformal to both the leading and trailing edges, so that a reasonable mesh spacing in the spanwise direction can be used with the resulting more gradual flow variations in the spanwise coordinate.

11

Setting $\bar{\varphi}(\xi,\eta,\zeta,t) = \varphi(x,y,z,t)$, Eq. (9) in the transformed plane assumes the form (see Appendix B)

$$(c\tilde{f_0})_t + (c\tilde{f_1})_\xi + (c\tilde{f_2})_\eta + (c\tilde{f_3})_\zeta = 0$$

$$\tilde{f_0} = -\sigma(\sigma\tilde{\varphi_t} + \frac{1}{c}\tilde{\varphi_\xi})$$

$$\tilde{f_1} = (\frac{K}{c^2} + M_\infty^{-2}\xi_y^2)\tilde{\varphi_\xi} + M_\infty^{-2}\xi_y\tilde{\varphi_\eta} - \frac{\sigma}{c}\tilde{\varphi_t} - (\frac{3}{2}\frac{1}{c}\xi_y^2 + \frac{B}{c^3})\varphi_\xi^2 - \frac{1}{2c}\varphi_\eta^2 - \frac{2\xi_y}{c}\tilde{\varphi_\xi}\tilde{\varphi_\eta} \qquad (11)$$

$$\tilde{f_2} = M_\infty^{-2}\xi_y\tilde{\varphi_\xi} + M_\infty^{-2}\tilde{\varphi_\eta} - \frac{1}{c}\xi_y\tilde{\varphi_\xi}^2 - \frac{1}{c}\tilde{\varphi_\xi}\tilde{\varphi_\eta}$$

$$\tilde{f_3} = M_\infty^{-2}\tilde{\varphi_\zeta} \qquad\qquad \xi_y = -\frac{1}{c}(x'_{LE} + \xi\, c')$$

Another less reliable approach with respect to the coordinate system was used by Schmidt, Rohlfs, and Vanino (Reference 8), which may warrant a reexamination for the unsteady case due to its simplicity. Here a cartesian coordinate system is used, but the mesh spacing in the y direction is adjusted such that the relative position of the leading edge relative to the local mesh is kept uniform over the span to moderate the consequences of using an inadequate mesh in the spanwise direction. Here the exact solution can be used in the steady case to tailor the mesh pattern. The advantage here will be the possibility of using the simpler Eq. (9) rather than the above Eq. (11).

4.0 WING BOUNDARY CONDITION

It is well known that in boundary value problems, the boundary conditions invariably play a key role. This is particularly the case for the unsteady transonic problem where the flow tangency condition on the wing serves as the driving or forcing function for the flow development.

12

At the surface of the wing defined by $B(\bar{R},T) = 0$ where $\bar{R}$ is the space vector $\bar{R}(X,Y,Z)$, the normal component of local flow velocity vector $(\nabla\Phi)$ relative to the moving surface element with velocity $\bar{V}_B$ must be zero. That is,

$$(\nabla\Phi - \bar{V}_B) \cdot \bar{N}_B = 0. \tag{12}$$

Here $\bar{N}_B$ is the instantaneous outward normal to the wing surface, $B(\bar{R},T)=0$, given by

$$\bar{N}_B = \frac{\nabla B}{|\nabla B|}$$

where the gradient ∇ operates only with $\bar{R}$.

Further, by differentiation, we have

$$\frac{dB}{dT} = B_T + \nabla B \cdot \frac{d\bar{R}}{dT} = B_T + \bar{V}_B \cdot \nabla B = 0$$

Replacing $\bar{V}_B$ by $\nabla\Phi$ in this equation using Eq. (12), we obtain the required boundary condition for the wing; that is

$$B_T + \nabla\Phi \cdot \nabla B = 0 \tag{13}$$

13

If we now introduce the perturbation potential and the nondimensional variables from Eq. (3) into Eq. (13) and retain only the lowest order terms in the perturbation potential, we obtain

$$\varphi_z(x,y,b^\circ,t) = \sigma\, b_t^\circ(x,y,t) + b_x^\circ(x,y,t)$$

where $B(X,Y,Z,T) = z - b^\circ(x,y,t)$.

Expanding φ_z in a Taylor series about $z = 0$, we obtain

$$\varphi_z(x,y,0,t) + \varphi_{zz}(x,y,0,t)\, b^\circ + \cdots = \sigma\, b_t^\circ + b_x^\circ \tag{14}$$

or to the lowest order

$$\varphi_z(x,y,0,t) = \sigma\, b_t^\circ + b_x^\circ \; . \tag{15}$$

Eq. (15) constitutes the important wing boundary condition.

It should be noted here that for wings with blunt leading edges, not only is the assumption of small perturbations invalid, but the neglected higher order terms of the Taylor expansion on the left side of Eq. (14) invariably overwhelm the retained lowest order term. Moreover, omission of these higher order terms also renders pure plunging motion degenerate for $\sigma \to 0$. Finally, note that the small disturbance approximation is violated if the time scaling σ is taken too large.

Consider next the important problem of the gust. Classically such a case was treated for example by simply imposing a moving step change of

14

the angle of attack. No doubt a measure of the gust loading can be obtained in this way, but it would be of importance to treat the gust in a more realistic manner, at the least, to assess the classical gust treatment. Thus for this purpose, a gust packet with a "typical" profile of upwash in both space and time is introduced into the flow at the far upstream boundary and allowed to convect downstream toward the wing. Here some experimentation is required to compensate for the diffusion of the gust packet, such that the desired gust is achieved just upstream of the wing. Such experimentation should be logically carried out in the planar case. Such an approach would parallel that carried out experimentally by M. Platzer of the Navy Postgraduate School who employed an unsteady jet flap upstream of the test model to generate a gust.

Finally, one must impose the important Kutta condition at the wing trailing edge which controls the local chordwise circulation and therefore the local shed rate of vorticity. That is, we have the requirement that as the trailing edge is approached along the upper and lower surfaces of the wing, the pressure approaches a common value. Thus we have the condition

$$[C_p] = C_p(x_{TE}, y, 0^+, t) - C_p(x_{TE}, y, 0^-, t) = 0 \qquad (16)$$

where $x = x_{TE}(y)$ defines the trailing edge and $z = 0+$, 0^- represent respectively the upper and lower surface of the wing; or using Eq. (10), we obtain for the Kutta condition,

$$\left(\frac{\partial}{\partial x} + \sigma \frac{\partial}{\partial t}\right)[\varphi] = 0 . \qquad (17)$$

5.0 TRAILING WAKE CONDITION

The physical picture as given by Helmholtz's vorticity law is that at a given point on the trailing edge, as the local chordwise circulation changes, the change in circulation must be shed into the flow at the trailing edge. Such shed vorticity is transferred to the fluid particle

15

in residence at the trailing edge at the time of the shedding, thereafter traveling downstream always tied to the fluid particle.

In an Eulerian representation, along the trailing vortex sheet, one must have a continuity of both streamline slope and pressure across the sheet. These conditions will be imposed, as in the wing tangency condition, in a quasi-planar fashion on the z = 0 plane. That is,

$$[\varphi_z] = \varphi_z(x,y,0^+,t) - \varphi_z(x,y,0^-,t) = 0 \tag{18}$$

and

$$[C_p] = C_p(x,y,0^+,t) - C_p(x,y,0^-,t) = 0 \, .$$

The second condition above can be reexpressed in terms of the perturbation potential using Eq. (10) as follows:

$$\left(\frac{\partial}{\partial x} + \sigma \frac{\partial}{\partial t}\right)[\varphi] = 0 \tag{19}$$

or in terms of the general integral

$$[\varphi(x,y,t)] = [\varphi(x-\sigma t, y)] \, .$$

The substantive or convective derivative in Eq. (19) indicates that the jump in φ generated at the trailing edge travels downstream along the particle path line at the particle speed $1/\sigma$ as required by the Helmholtz vortex law. (Note here that the apparent distortion of the particle speed is due to the change of scale of the time introduced in Eq. (3).) Thus the $[\varphi]$ to be assigned at a point $x - x_{TE} = x_0$ downstream of the trailing edge at $t = t_0$ is that which was shed at the trailing edge at the earlier time $t = t_0 - x_0 \sigma$.

16

As $\sigma \to 0$ (low unsteadiness or in the low frequency limit in the case of harmonically oscillating flow), we have $[\varphi(x, y, t)] = [\varphi(x_{TE}, y)]$. That is, $[\varphi]$ for a given y and t along the wake is invariant with x at the value at the trailing edge. In this "low frequency" limit, the flow changes so slowly that in the time required for the shed vorticity to travel far downstream, the flow, in particular the $[\varphi]$ at the wing trailing edge, has not significantly changed.

6.0 OUTER BOUNDARY CONDITIONS

The far field conditions for the unsteady 3D problem are that sufficiently far upstream and laterally from the wing, the flow must approach the freestream conditions, while far downstream it must approach a Trefftz type flow, characterized by the trailing vortex system. In a calculational procedure, outer boundaries at finite but large distances from the wing must be used, and the question then arises as to what conditions to prescribe on such computational boundaries.

To answer this question, let us first recall that in the case of unsteady 3D flow, we have a hyperbolic problem. Thus, for example, the "Mach cone" for the low frequency planar case is given in Figure 4 from Reference 9. Guidance as to the necessary far field condition for the unsteady 3D case can thus be obtained by examining the simplified case of a steady supersonic flow over an axial symmetric body shown in Figure 5. Here the lines abc, cb"d, bef, and eb" are characteristics or Mach waves. Thus if we take an outer boundary no closer to the body than c'cc", one can determine the flow at the body independent of the condition prescribed along cc". We can for example set the flow slope $\varphi_n = 0$ along the boundary c'cc". If, however, we take the closer boundary b'bb", then the flow along fd on the body will be distorted from the correct flow unless the right condition is prescribed along bb" of the outer boundary. In the past a condition along bb" has been sought assuming some form of an "outgoing wave" or radiating condition. It is clear that such an approach cannot be strictly exact since the flow along bb" is clearly dependent not only on the initial values along be, but on the characteristic initial values along bc, beyond the outer boundary bb". On the other hand, if the

boundary b'bb" is located sufficiently remote from the body, a condition such as the above outgoing wave condition or the simpler condition $\varphi_n = 0$ (solid wall condition) can be prescribed without serious errors being reflected back onto the body along the segment fd.

Thus in the present unsteady 3D transonic problem we shall prescribe the condition $\varphi_n = 0$ on the lateral boundaries taken sufficiently far from the wing that either the reflected perturbations do not have sufficient time to impinge back onto the wing, or if they do, the reflected errors are negligible. This can be easily verified in the calculations by successively extending the boundaries outward until the desired result is achieved. Frequently mesh stretching is used to extend the location of the outer boundaries. Here an additional source of error can arise if the stretched mesh is no longer able to resolve properly the outgoing unsteady waves, but in general such an error probably will not have a significant effect in the above circumstances.

The far downstream boundary condition requires special consideration since the flow in the far downstream boundary is affected by the unsteady trailing vortex sheet passing through it. (See Figure 6.) If the downstream boundary is taken sufficiently far from the wing, the flow in the downstream boundary will be independent of the influence of the wing and will be a function only of the trailing vortex sheet fluxing through it with frozen vorticity traveling at the propagation speed $1/\sigma$. (See Section 5.0) That is, the flow in a plane transverse to the freestream moving at the velocity $1/\sigma$ will be invariant with time, that is $\varphi(x,y,z,t) = \varphi(t-\sigma x, y)$, or

$$\left(\frac{\partial}{\partial x} + \sigma \frac{\partial}{\partial t}\right)\varphi = 0 . \tag{20}$$

This then is the condition to be prescribed on the far downstream boundary, and it is equivalent to $C_p = 0$. In the limit $\sigma \to 0$, this condition reduces to $\varphi_x = 0$.

18

Finally note that if the downstream boundary is not taken sufficiently far downstream, the effect of the wing cannot be ignored, and the flow in a plane transverse to the freestream, traveling downstream at a velocity of $1/\sigma$, will not be invariant with time. In such a case, the use of a boundary condition such as Eq. (20) in a computation could lead to numerical errors or instabilities if the proper outfluxing of the trailing vorticity is not allowed.

7.0 VENTILATED WIND TUNNEL WALL CONDITIONS

In the present section we shall review the wall boundary conditions for a ventilated wind tunnel with slotted or perforated walls. The conditions for the slotted wall are given, for example, in Reference 10; while those for the perforated walls are given in Reference 11. These conditions understandably are highly idealized, and their validity has yet to be demonstrated in the steady case in a real wind tunnel environment. These conditions will be extrapolated to the unsteady case by assuming their applicability to the instantaneous flows.

7.1 Slotted Wall

The idealized condition for the slotted wall is based on the assumption that the pressure at the slot is equal to the plenum pressure, while the normal velocity is zero along the solid portion of the wall. These mixed conditions are converted to a homogenized condition applicable on a substitute boundary just interior to the actual walls. This condition is derived by applying the conservation of mass between the actual and substitute boundaries assuming the streamwise variation of the flow to be negligible. In the usual case that the spacing d between the slots is large relative to the slot width, and with the plenum pressure set equal to the freestream pressure, one obtains the slotted wall condition

$$C_{P,w} = K \frac{\partial \theta_w}{\partial x} \cong K \varphi_{xz} . \tag{21}$$

19

Here $C_{p,w}$ and θ_w are the pressure coefficient and the streamline slope on the substitute boundary, which can be taken at the actual wall location; and K is a constant dependent only on the slot configuration. In the 3D case θ_w is the slope of the streamline in a streamwise plane normal to the wall. The primary source of error in the derivation of the above condition is the assumption of inviscid flow.

The above condition is valid only along those portions of the wall where an outflow from the tunnel to the plenum occurs. When an inflow occurs, the total pressure of the incoming air has suffered a drop due to the mixing of the moving tunnel air with the stagnated plenum air. In this case in Reference 10 an alternate condition was derived, again with simplifying assumptions, given by

$$C_{p,w} - K' \varphi_{xz} = C_{p,\text{plenum}} \tag{22}$$

Here $C_{p,\text{plenum}}$ is the plenum pressure coefficient assumed as constant, and K' is the essentially constant perturbation potential at the slot.

In the unsteady case we assume that Eqs. (21) and (22) apply to the instantaneous flow, setting

$$C_p = -2(\varphi_x + \sigma \varphi_t).$$

The outstanding problem with these ideal slotted wall conditions is the selection of the constants K and K' since in a lifting case, both outflow as well as inflow can be expected. Moreover, one faces the physically unreasonable discontinuity of the boundary condition as the wall flow switches between an inflow and an outflow.

Understandably, in steady wall interference studies, the outflow condition Eq. (21) is usually assumed to prevail along the entire wall, so that only the tunnel dependent K is needed.

20

Theoretical as well as experimental derivations of K have been reviewed by Barnwell (Reference 10) who also recommended values of K as a function of the ratio of the width to spacing of the slots.

7.2 Perforated Wall

The basis of the perforated wall condition is that the mass flux through the wall is proportional to the pressure difference across the wall. This then leads to the perforated wall condition

$$C_{p,w} = -2(\varphi_x + \sigma \varphi_t) = \frac{1}{R} \varphi_z \qquad (23)$$

Here the plenum pressure has been set equal to the freestream pressure, and the constant R is a measure of the wall porosity. The parameter R is usually determined in a laboratory setup by measuring the mass flux through the perforated plate as a function of the pressure drop across the plate without an ambient flow along the plate. How applicable such a determination of R is for the case of the wind tunnel wall is not clear, since in the latter, one has a complex boundary layer flow passing transversely across the perforations.

As for the slotted wall, Eq. (23) no longer applies in the case of inflow from the plenum to the tunnel. Here again the inflow has a greatly reduced total pressure (approximately equal to the plenum pressure), and this low energy air then forms a buffer layer along the wall that softens the wall effect. Some consequences of this are discussed in Reference 12.

Clearly the effects of this low energy buffer layer are difficult to assess, so that the outflow condition (23) is usually assumed to apply over the entire wall. Mokry (Reference 11) found that improved prediction of the wall interference is obtained if a different value of R is used for the upper and lower walls, somewhat compensating for the less accurate treatment of the inflow.

21

7.3 Summary of the Wall Boundary Conditions

There is no question that the ventilated wall conditions given above are idealized conditions that hopefully yield the "first order" effects of the wall interference. In summary we have therefore the following wall conditions.

Slotted Wall:

$$2(\varphi_x + \sigma \varphi_t) + K \varphi_{x\underline{z}} = 0$$

where K is the slot parameter given, for example, in Figure 4 of Reference 10.

Perforated Wall:

$$2(\varphi_x + \sigma \varphi_t) + \frac{1}{R} \varphi_z = 0$$

where typical values of the porosity R are given in Reference 13.

For completeness we have

Solid Wall:

$$\varphi_z = 0$$

Free Jet:

$$\varphi_x + \sigma \varphi_t = 0$$

Side walls of the wind tunnel are usually closed walls, so that the condition $\varphi_y = 0$ is prescribed on these walls.

7.4 Wind Tunnel Wall Interference

Assuming that the ventilated wall conditions given above are valid,

22

wall interference is obtained by comparing the computational results with the wall condition and with an infinite freestream condition. If experimental pressure distribution data are available in the wind tunnel of interest, they can be used to determine the wall parameters.

In using experimental results in this fashion, one must check that the test section length, both upstream and downstream of the wing, is sufficiently large that the effects of the wing have subsided sufficiently that freestream conditions prevail at the extremities of the test section. In particular an erroneous determination of the freestream Mach number can arise if the upstream effects of the wing have not sufficiently attenuated where the measurement for the freestream velocity is taken.

Finally, we shall review the resonant wall interference that arises in unsteady testing which can significantly distort, for example, the results in flutter testing. Here the unsteady waves generated by the wing resonate between the wing and the wind tunnel wall at discrete frequencies that are functions of the velocity of sound and the ratio of the tunnel height to wing chord. A typical wind tunnel result showing these interference effects from Reference 14 is shown in Figure 7 for the case of the pitching oscillation of the NACA 65-010 airfoil. Here it is seen at the resonant frequency that the amplitude of the lift and moment variations drops abruptly, while a large phase lag increase is seen carrying over an extended range of frequencies below resonance. The results of Reference 14 further showed the resonant frequency fell in the low frequency range that is relevent to the flutter phenomena.

The above results are for a planar wing in subcritical flow with solid wind tunnel walls. Thus in the unsteady testing of a swept wing in the supercritical range with ventilated wind tunnel walls, the possibility of such resonant wall interference must be kept in mind. Of particular importance is the possible large distortion of the phase which may be present well below the resonant frequency where the distortion of the lift and moment amplitudes is not evident. Here the calculational procedure

23

based on the unsteady transonic 3D problem formulated in the previous sections would be invaluable to check and correct for the above resonant wall interference. Viscous interaction effects, to be described in Section 10, must be incorporated into these calculations.

8.0 SUMMARY OF THE PROBLEM FORMULATION

The purpose of the present section is to summarize the initial-boundary value problem in the small disturbance limit derived in detail in the previous sections and to define several limiting cases.

Thus the general flow equation for the perturbation potential is

$$-\sigma(\sigma\varphi_t + 2\varphi_x)_t + (\beta^2\varphi_x - A\varphi_x^2 - \tfrac{1}{2}\varphi_y^2)_x + M_\infty^{-2}[(1-M_\infty^2\varphi_x)\varphi_y]_y + M_\infty^{-2}(\varphi_z)_z = 0$$

where

$$\beta^2 = \frac{1-M_\infty^2}{M_\infty^2} \qquad A = \tfrac{1}{2}(\gamma+1)\left[1-\left(\frac{\gamma-2}{\gamma+1}\right)(1-M_\infty^2)\right].$$

The significance of the underlining will be discussed shortly. The pressure coefficient is

$$c_p = -2(\varphi_x + \sigma\varphi_t).$$

The boundary condition on the wing $(z = b^\circ(x,y,t))$ is

$$\varphi_z(x,y,0^\pm,t) = b_x^\circ(x,y,t) + \sigma\, b_t^\circ(x,y,t)$$

Additionally the Kutta condition

$$\left(\frac{\partial}{\partial x} + \sigma\frac{\partial}{\partial t}\right)[\varphi(y,t)] = 0$$

24

is imposed at the subsonic trailing edges.

Along the trailing vortex sheet we have the conditions

$$[\varphi_z] = 0$$

$$\left(\frac{\partial}{\partial x} + \sigma \frac{\partial}{\partial t}\right)[\varphi] = 0$$

Finally for the outer conditions on boundaries taken sufficiently far from the wing, we have,

$$\varphi = 0 \qquad \text{(far upstream and far laterally)}$$

$$\left(\frac{\partial}{\partial x} + \sigma \frac{\partial}{\partial t}\right)\varphi = 0 \qquad \text{(far downstream)}$$

To complete the formulation, an initial starting flow must be prescribed, which can be taken as any readily available steady flow or the uniform flow $\varphi = 0$ if such a flow is unavailable.

There are several limiting cases of the above problem. In the limit that $\sigma \to 0$, we have the fluid mechanically defined quasi-steady flow in which terms underlined by the solid line in the above equations are deleted. Here the time appears only parametrically in the wing condition.

There is also the quasi-steady problem as defined by the aeroelastician. Here the time derivatives in the flow equation are deleted, but they are retained in all the other equations.

We can next define the low unsteadiness problem in which the terms underlined by the dashed lines are deleted. Here the unsteadiness is manifested only through the φ_{xt} term in the potential equation, and implicitly in a parametric fashion through the wing boundary condition.

25

Finally, we can define a quasi-high unsteadiness problem in which only the φ_{tt} term is deleted in the potential equation with all time derivatives retained in the other equations.

What are now the implications and significances of the above various limiting cases? For the general case including the gust problem, no terms in the above formulation can be deleted. Moreover, solutions to the complete problem are essential to establish the range of validity of the approximate cases defined above, in particular to establish upper bounds on the permissible values of σ.

The quasi-high unsteadiness case is of particular interest. Here the addition of the time derivatives in the boundary conditions can be easily implemented in the low unsteadiness case, to then extend the range of applicability to cover most of the unsteady cases of interest except for the gust problem. (Preliminary results of van der Vooren of the NLR.)

It is appropriate finally to comment on the simplified approach not considered above in which the unsteadiness is considered as a small perturbation about a steady background flow. Such a linearized unsteady approach is undoubtedly meaningful so long as significant shock waves or more precisely their significant motion do not arise. Clearly, if one considers the region of the flow including the wing surface traversed by the shocks, the unsteadiness here cannot be considered a small perturbation since the flow changes abruptly from a supersonic to subsonic flow (or vice versa) as the shock travels over points of such a subdomain.

It may be recalled that the expected transonic aeroelastic problems are aggravated by the magnified lift and moment changes due to the motion of shock waves, most probably to the phase lags between the shock motion and the wing motion. There simply is no possibility to capture the shock motion correctly with the above time linearized approach.

In a similar vein, there have been serious queries regarding the possibility that the flow for a wing in combined plunging and pitching oscillatory motions can be considered as a superposition of the flow with a pure plunging motion and a pure pitching oscillation. Again if significant shock motion arises, the flow is essentially nonlinear, precluding such a superposition.

SECTION IV
LIMITATIONS OF AND COMPENSATION FOR THE SMALL DISTURBANCE APPROXIMATION

The nature of the errors caused by the small disturbance approximation in the unsteady case can be directly extrapolated from the steady case which has been extensively studied. Thus at blunt leading edges, not only is the small disturbance potential equation inaccurate, but the tangency condition is grossly in error as well as the quasi-planar fashion in which it is imposed. Here the important consequence is, not the inaccuracy about the stagnation point, but the accuracy of the subsequent upper surface leading edge expansion to supersonic velocities. This establishes the suction plateau and hence the strength of the shock waves. Elsewhere on the wing where the surface slopes become excessive as at large values of the angle of attack or in the aft camber region of supercritical airfoils at low or moderate angle of attack, significant errors can also arise.

In the unsteady case of a swept wing, there is a simple means to compensate for these inaccuracies (Reference 15). Here the steady exact flow over a suitably selected representative planar airfoil or the 3D wing itself can be used to fashion shape changes in the nose or aft camber regions of the wing to compensate for these shortcomings.

Thus consider a swept wing with a moderate sweep ($\sim$30°) with a supercritical airfoil section. First a characteristic planar flow is defined at the midsemispan using local sweep theory and assuming uniform downwash. This 2D flow is then computed by an existing exact potential method. The 2D small disturbance code is then used, distorting the nose slopes in a smooth fashion as with the Riegels rule (Reference 16) and adding aft decambering ramp, such that the exact pressures are obtained. If the 2D small disturbance code has a capability to prescribe pressures in lieu of the surface slopes, the latter aft decambering ramps can be evolved directly by prescribing the exact pressures in the aft portion of the upper and lower surfaces.

28

The airfoil shape changes thus evolved are then suitably incorporated into the swept wing. Clearly some development is required in the technique, using the exact 3D flow as a validation base. In the case of a rigid body pitching oscillation case, the above shape tailoring would be carried out at the mean angle of attack.

It is clearly not the intent of the above procedure to obtain a "perfect" compensation for the instantaneous pressure distributions. It is desirable, however, to obtain an acceptable prediction of the shock motion and the resulting lift and moment time histories acceptable for aeroelastic applications.

SECTION V
TURBULENT VISCOUS INTERACTIONS

In the present section we shall review the important viscous interactions for the unsteady transonic flow over wings of moderate sweep. Since there is little data available for the unsteady case, we must therefore extrapolate our experiences with steady flows. We shall then describe two methods to incorporate these viscous interactions into the inviscid flow methods. They are the viscous ramp method (Reference 17) and the Lag Entrainment method (References 18 and 19), which have been selected for their ability to predict the important viscous effects without intolerably complicating the overall procedure.

For swept wings of moderate sweep ($\lesssim 30^\circ$) and aspect ratios in the range of five or greater, we shall postulate that the viscous interactions can be treated in a suitable quasi-planar fashion in cuts normal to the sweep. That this is a reasonable approximation can be seen in Figure 8 for the case of a yawed wing of constant chord and infinite aspect ratio of 35° sweep tested by Elsenaar, van den Berg, and Lindhout (Reference 20). Here it is seen that the displacement thickness computed in the above quasi-planar way closely approximates the 3D calculations with McLean's method (Reference 21). Also seen here is the inappropriateness of taking cuts in the streamwise direction. Similar results were obtained by Nash and Tseng (Reference 22). The above approximation should be acceptable over most of the wing, except in the tip region, when severe separation is absent. With severe separation, particularly near the trailing edge, a spanwise flow of the "dead air" occurs greatly increasing the viscous displacement in the tipward direction, thereby invalidating the quasi-planar model.

In planar unsteady flows, it has been made plausible in Reference 17 that the important viscous interactions for sufficiently moderate unsteadiness can be treated in a quasi-steady way in a suitable framework. (We shall review this in more detail shortly.) Thus a discription of the viscous interactions in the steady planar case will be relevant.

30

In Figure 9 we compare schematically the flows over a supercritical airfoil and the corresponding pressure distributions for the case of inviscid and viscous flows. The dominant and well known effect of viscosity shown here is the reduction of the shock pressure rise and the consequent upstream displacement of the shock in the viscous case relative to the inviscid case. Here the reduction of the viscous shock pressure rise is due to the abrupt increase of the boundary layer displacement (a wedging effect) just downstream of the shock which converts the normal shock in the inviscid case to the observed weaker oblique shock with its reduced pressure rise. The wedging displacement at the shock is the consequence of the severe reduction of the fullness of the boundary layer velocity profile and increase of the boundary layer thickness after passage through the abrupt shock adverse pressure gradient. The reduced shock pressure rise then displaces the shock upstream.

A second effect of viscosity also shown here is the reduction of the plateau loading caused by the aft decambering effect of the boundary layer and near wake. This effect is particularly significant in the case of aft cambered airfoils since the resulting aft decambering has a global influence on the pressure distribution as shown above.

In summary, the primary viscous effect is the shock-boundary layer interaction. For aft cambered airfoils, additionally the aft displacement effects of the boundary layer and near wake will be important. An acceptable determination of the lift and moment on the wing cannot be made without incorporating these effects.

Two methods to calculate the above viscous effects for the unsteady 3D case are the viscous ramp method and the lag entrainment method. These methods are essentially planar steady methods. They will be relevent for the 3D unsteady case since, as described earlier, a quasi 2D flow is postulated and the resulting planar flows then considered quasi-steady in the proper framework. These methods have been selected for their simplicity for near-term applicability.

31

1.0 The Viscous Ramp Method

This procedure is a phenomenological method in which a priori determined shape changes simulating the viscous displacement effects are incorporated into the inviscid procedure. Here the shock-boundary layer interaction is modeled by placing a wedge-nosed ramp at the base of the shock to obtain the reduced shock pressure rise. The appropriate wedge angle is determined via the shock polar using a postulated post-shock pressure based upon measurements. (See Figure 10.) Other features of the wedge ramp as well as its placement relative to the shock profile are developed by calculations using as a comparison base suitable steady measured pressure distributions. Models of such ramps for example have been developed by Murman (Reference 23) who used the shock detachment value of the wedge angle, and in Reference 17.

In the unsteady case, the shock in general will be out of phase with the motion of the airfoil. Thus the wedge ramp must be tied, not to the instantaneous angle of attack, but to the prevailing shock, with the wedge angle adjusting instantaneously to the instantaneous shock strength. In other words the boundary layer just downstream of the shock, and hence the wedge ramp, is assumed to equilibrate in a time sufficiently short that the shock does not change significantly in position or strength. This approximation is not unreasonable provided the flow unsteadiness is not excessive. Thus consider the pitching oscillation case with the reduced frequency k = 0.468 treated in Reference 17. Here the characteristic time for the unsteadiness of the flow, and hence that of the shock motion, is the period of the oscillation, which in the above case is $13.4\,\tau_0$, where τ_0 is the time required for the airfoil to travel one chord at the freestream velocity. On the other hand the characteristic time for the equilibration of the boundary layer just downstream of the shock to the changing shock should be no greater than one τ_0. Thus we can tailor the wedge ramp to the instantaneous shock in a quasi-steady fashion.

Consider next the aft displacement effects of the boundary layer and the near wake. These effects are less dramatic than those of the

32

shock-boundary layer interaction, but nevertheless they still can play an important role, even affecting the shock motion by modifying the pressures upstream of the shock. In an unsteady case, the aft pressure gradients determining the boundary layer displacement are closely in phase with the instantaneous angle of attack. We shall therefore incorporate the aft viscous ramps in a quasi-steady fashion to the instantaneous angle of attack.

The shaping of the aft ramps will be carried out in a steady flow at a characteristic angle of attack for the unsteady flow. Thus in the case of the pitching oscillation, the mean angle of attack will be used. For this purpose the steady experimental pressure distribution for the airfoil at the appropriate Mach number and Reynolds number is required. The shaping of the aft ramps is then determined by an inviscid calculation in which the measured pressures are prescribed as boundary condition in lieu of the surface slopes. The results will yield aft shape changes required to yield the measured pressures, the latter incorporating the effects of the boundary layer as well as the near wake. The resulting aft ramps are then frozen onto the airfoil. They will then be off-design at angles of attack other than the mean value, but the errors will be assumed tolerable since variations of the aft pressure gradients, or more precisely their effect on the boundary layer displacement, are usually not large.

The above decoupled treatment of the viscous interactions at the shock and in the aft region is permitted only when the Reynolds number is sufficiently high that the type B interaction defined by Pearcey (Reference 24) does not arise. That is, the boundary layer is sufficiently thin that it recovers from its encounter with the shock adverse pressure gradient prior to its encounter with the second aft adverse subcritical pressure recovery. Without a full recovery of the loss of the velocity profile fullness through the shock before encountering the second adverse gradient, the effects of the latter are greatly magnified, precluding the assumed decoupled treatment of the separate interactions.

33

In addition, if the boundary layer thickness upstream of the shock is "unnaturally" large, for example, as the result of an overly conservative tripping of the boundary layer in a wind tunnel test, a type B interaction can also arise if the increase of the thickness of the recovered boundary layer is sufficiently large.

The above viscous ramp procedure consequently reduces to the computation of an inviscid flow with a priori determinable time dependent shape changes. In the case of the wedge-nosed ramp for the shock-boundary layer interaction, when the Mach number upstream of the shock is 1.25, the wedge angle corresponds, in the case of the shock detachment angle, to approximately 5.3o. The movement of such a wedge ramp on the surface of the airfoil creates a significant disturbance to the highly sensitive flow. Thus in the implementation of the viscous ramp procedure into a numerical procedure, skill must be exercised to avoid numerical instabilities and excessive additional computing time.

2.0 Lag Entrainment Method

The viscous ramp method described above is a phenomenological procedure, devoid of differential equations, requiring minimal additional computing time for near-term use. A more refined procedure will require appropriate flow differential equations to describe the viscous flow, and such equations must be able to treat shock-boundary layer interactions and locally separated flows in a reasonable fashion. The turbulent transport model applicable for such flows are presently not available, and prospects for their development are discouraging. We must therefore select the level of description of the viscous flow such that this shortcoming can be most simply circumvented in a phenomenological manner. We must further continually keep in mind the requirement of minimal computing times. Since we shall consider the 3D unsteady flow to be quasi 2D, and the latter quasi-steady, we need consider only the steady 2D case. These considerations then lead naturally to integral

34

methods with ordinary differential equations, rather than partial differential equation methods; in particular to the lag entrainment methods which have had success in previous steady 2D cases (see References 18, 19 and 25).

In treating the viscous interactions with the integral equation method, one considers the δ^*, the viscous displacement, a quantity required to input directly the viscous effects into the inviscid procedure. However, for the concept of the displacement thickness to be strictly meaningful, the pressure must be invariant across the viscous layer. Such an assumption is most probably violated in the region of the shock impingement and about the trailing edge where the boundary layer passes into the wake. To circumvent this conceptual difficulty, we shall define a fictitious boundary layer for which the concept of δ^* is meaningful, tailoring the necessary empirical inputs for the turbulent transport to fit the framework of this substitute boundary layer.

The starting point for the lag entrainment method is the integral form of the streamwise momentum and the continuity equations obtained by an integration across the boundary layer; that is,

Streamwise momentum:

$$\frac{d\theta}{dx} + (H + 2 - M_e^2) \frac{\theta}{U_e} \frac{dU_e}{dx} = \frac{1}{2} C_f$$

(24)

Continuity:

$$\frac{d}{dx} [\rho_e U_e (\delta - \delta^*)] = \frac{V_e}{U_e} \equiv C_E$$

(25)

35

Here x is the streamwise coordinate; U_e the streamwise velocity, V_e the transverse velocity, and ρ_e the density all at the outer edge of the boundary layer; the displacement or mass flux defect thickness is defined by

$$\delta^* = \int_0^\delta \left(1 - \frac{\rho U}{\rho_e U_e}\right) dy$$

where δ is the boundary layer thickness; the momentum thickness is defined by

$$\theta = \int_0^\delta \frac{\rho U}{\rho_e U_e}\left(1 - \frac{U}{U_e}\right) dy$$

the form factor $H = \delta^*/\theta$; and $C_f = \tau_w \left(\frac{1}{2}\rho_e U_e^2\right)^{-1}$ is the wall skin friction coefficient. For convenience, the above lengths are nondimensionalized by the wing chord, the velocities by the freestream velocity, and the density by its freestream value. Note also that the velocities are not perturbations.

Eqs. (24) and (25) contain the six unknowns δ, δ^*, θ, U_e, V_e and C_f. (Here M_e and ρ_e are obtained from U_e from the isentropic relations.) For a fully determined set of equations, four additional supplementary equations are required. These are furnished by a skin friction law, by defining a two parameter velocity profile law, and by a lag entrainment hypothesis furnished by Bradshaw (Reference 26). The final required equation is furnished from the interaction with the outer inviscid flow. These auxiliary relations are next discussed.

36

For the skin friction law, several forms have proven to be satisfactory. Thus, for example, in References 19 and 22, the Spaulding-Chi law was used, while in Reference 18, the Ludwieg-Tillmann formulae has been used. These laws are given in the functional form

$$C_f = C_f(M_e, R_\theta, H) \tag{26}$$

where R_θ is the local Reynolds number based upon θ, the momentum thickness.

For the velocity profiles we shall assume the two parameter family developed in Reference 27, which was shown to be adequate to represent the diverse range of profiles measured by Seddon (Reference 28) for the case of the normal shock impingement on the turbulent boundary layer along a flat plate. Here Cole's law of the wake is used together with van Driest's law of the wall with a laminar sublayer. Using the Crocco-Busemann law for zero heat transfer to express the density profile in terms of the above velocity profile, one can obtain the displacement and momentum thicknesses in terms of the two parameters δ and C_f; that is,

$$\delta^* = \delta^*(\delta, C_f) \qquad\qquad \theta = \theta(\delta, C_f) \tag{27}$$

$C_E = V_e/U_e$ in Eq. (25) is defined as the entrainment coefficient which is equal to the slope of the streamline of the inviscid flow just entering the boundary layer. It is a measure of the rate at which outer inviscid flow is being entrained locally into the boundary layer. Its introduction into the boundary layer analysis was first due to Head (Reference 29).

For the skin friction law, several forms have proven to be satisfactory. Thus, for example, in References 19 and 22, the Spaulding-Chi law was used, while in Reference 18, the Ludwieg-Tillmann formulae has been used. These laws are given in the functional form

$$C_f = C_f(M_e, R_\theta, H) \tag{26}$$

where R_θ is the local Reynolds number based upon θ, the momentum thickness.

For the velocity profiles we shall assume the two parameter family developed in Reference 27, which was shown to be adequate to represent the diverse range of profiles measured by Seddon (Reference 28) for the case of the normal shock impingement on the turbulent boundary layer along a flat plate. Here Cole's law of the wake is used together with van Driest's law of the wall with a laminar sublayer. Using the Crocco-Busemann law for zero heat transfer to express the density profile in terms of the above velocity profile, one can obtain the displacement and momentum thicknesses in terms of the two parameters δ and C_f; that is,

$$\delta^* = \delta^*(\delta, C_f) \qquad \theta = \theta(\delta, C_f) \tag{27}$$

$C_E = V_e/U_e$ in Eq. (25) is defined as the entrainment coefficient which is equal to the slope of the streamline of the inviscid flow just entering the boundary layer. It is a measure of the rate at which outer inviscid flow is being entrained locally into the boundary layer. Its introduction into the boundary layer analysis was first due to Head (Reference 29).

37

Bradshaw (Reference 26) empirically related the entrainment coefficient functionally with the maximum shear stress within the local boundary layer profile by the relation

$$C_E = 10 \frac{\tau_{max}}{\rho_e U_e^2} \tag{28}$$

Prior history effects in the turbulent entrainment are incorporated by assuming a simple lag entrainment equation, which in Reference 18 is given by

$$\frac{d}{dx}\left(\frac{\tau_{max}}{\rho_e}\right) = \frac{\lambda}{\delta}\left(\frac{\tau_{max,eq}}{\rho_e} - \frac{\tau_{max}}{\rho_e}\right) \tag{29}$$

Here λ is a lag constant to be empirically determined, and $\tau_{max,eq}$ is the maximum shear stress for the equilibrium boundary layer in which the velocity and shear stress profiles are invariant with x.

To determine the maximum shear stress from the postulated velocity profile, in Reference 18 an eddy diffusivity is assumed. Though the maximum shear stress can be determined once the eddy diffusivity and the velocity profile are assumed, in Reference 18 an empirically determined location of the maximum shear stress within the profile is used, which is different for attached and separated flows. The resulting expressions for the equilibrium case are given in Figure 7 of Reference 18.

Finally U_e or δ^* is obtained from the inviscid flow. When U_e is furnished by the inviscid flow, a direct problem for the boundary layer is defined for which the separation point, $C_f = 0$, is a singular point. When the δ^* is inputed, an indirect problem is defined, but now the separation point is no longer a singular point. Quite clearly the latter formulation for the boundary layer is preferred.

38

Thus in summary, Eqs. (24)-(29), and an input of U_e or $d\delta^*/dx$ or δ^* from the inviscid flow calculations constitute the system of equations for the boundary layer, in particular the formulation from Reference 18. Green in Reference 19 proposed a similar lag entrainment procedure which differed from the above primarily in the expressions for the lag entrainment and in the choice of the velocity profile. Empiricism has been incorporated in the two methods in different ways, so that a direct comparison cannot be made without comparing the results for specific cases.

The validity of Green's lag entrainment method has been examined in Reference 25 for a number of cases by comparisons with experiments. In particular in Figure 11 we reproduce one of the shock-boundary layer interaction cases of interest, namely that tested by Seddon (Reference 28) for the normal shock impingement on a flat plate. Seddon measured the velocity profiles and the surface pressures and from these determined all of the dependent terms arising in Green's equations. In the results of Figure 11, Green's method was used to calculate M_e, θ, and C_f inputing the measured δ^*. The computed quantities are then compared with Seddon's experimental results in Figure 10. The agreement of θ and C_f are near perfect, with the main discrepancy arising in the post-shock recovery of M_e. Most plausible cause for the latter discrepancy is the displacement effects of the side wall boundary layers which were not removed. Similar good agreements with experiments were obtained for other cases.

In the above indirect problem for the boundary layer, where δ^* is inputed from the inviscid flow, it has been demonstrated that Green's equations can be integrated in a stable fashion through the shock pressure rise without difficulty. These are encouraging results that recommend the use of the lag entrainment methods.

3.0 Viscid-Inviscid Flow Coupling

In the previous sections we have formulated the problems for the inviscid flow and the boundary layer flow. We must next consider the

coupling of these two flows. In the classical low speed case, this was accomplished by the well known weak interaction iterative procedure. The starting point for the iteration is an inviscid calculation from which the surface pressure distribution required for the boundary layer calculation is obtained. The latter calculation then determines the displacement thickness which, when added to the original airfoil shape, results in a new effective airfoil shape and a new starting point. The above procedure is repeated until an invariant pressure distribution is obtained.

In the low speed case the convergence of the iteration is usually rapid so long as significant separation does not arise. With separation, a strong interaction arises requiring the boundary layer and the inviscid flow to be treated simultaneously.

The viscous interaction in the case of the supercritical flow over airfoils is an extreme case of a strong interaction. However, due to the extremeness of the shock-boundary layer interaction and the sensitivity of the transonic inviscid flow, in general, to perturbations of the surface boundary condition, a direct coupling alone may not preclude stability difficulties in the resulting numerical procedure.

The problem of the transonic coupling has been considered, for example, by Le Balleur (Reference 30) who treated the outer inviscid flow with a steady small disturbance relaxation procedure and the boundary layer with an integral method. A semi-inverse iterative procedure with under-relaxation was employed for the coupling where the inviscid flow was treated as a direct problem (surface slope prescribed to yield the pressure) and the boundary layer treated as an indirect problem (δ^* or slope prescribed to yield the pressure).

The iterative procedure was as follows. With an initial slope distribution given, the pressure distribution was computed for both flows. The difference of the resulting pressure distributions was then

used as a forcing function to evolve a slope correction by an approximate locally linearized procedure, the correction then suitably under-relaxed to serve as a new point of departure.

The movement of the resulting viscous ramp across mesh points from iteration to iteration in the above direct formulation of the inviscid problem undoubtedly strains the stability of the inviscid flow algorithm. This was relieved by Le Balleur who embedded a highly refined mesh about the shock which moved with the shock. Thus in this way with a moving mesh a given surface mesh point is spared the sudden confrontation with a large change of the boundary condition, as would arise in the case of a point in a fixed mesh when the viscous wedge moved onto it.

For the unsteady problem, the procedure of Le Balleur has the undesirable feature of increased computing times due to the need of a highly refined moving mesh about the shock and the need to iterate at each time step to achieve a time-accurate solution.

One has the further deficiency that the inviscid flow relaxation procedure is incapable of treating the shock profile region due to the large truncation errors. The consequent large numerical dissipative effects are primarily responsible for the shock profile. In Le Balleur's result near the surface the concavity of the δ^* surface widened the shock profile over many more mesh points than the customary three or so that would usually prevail and which must prevail outside the region of influence of the δ^* concavity. In the above widened portion of the shock profile, the use of a refined mesh has undoubtedly reduced the truncation errors, but one must then question the validity of the small disturbance equation in this region.

In the following we shall suggest an alternate procedure in an attempt to circumvent the above objections, coupling directly the inviscid and boundary layer flows. The shock profile region is then treated by an ad hoc procedure in which a bridging condition for the boundary layer is obtained to apply across the shock profile region.

41

Consider the low frequency case where the LTRAN 2 code developed by Ballhaus and Goorjian (Reference 31) may be used for the inviscid flow. This method employs a two step implicit approximate factorization difference algorithm in which the first step is a predictor step with the time and x (streamwise) derivatives treated implicitly and the y derivative treated explicitly. In this step (the x-sweep) the value of the potential along a given row of mesh points is determined simultaneously imposing the far upstream and downstream boundary conditions.

In the second step, the corrector step, corrections to the potential obtained in the x-sweep are obtained by treating the time and y derivatives implicitly in y-sweeps, imposing timely conditions along the airfoil.

For the boundary layer, the steady lag entrainment method will be used assuming the boundary layer to be quasi-steady relative to the instantaneous inviscid flow.

Formally a simultaneous coupling of the inviscid and boundary layer flows is first accomplished in the following way using Figure 12. Here we show the pressure distribution at the prior time (top), the inviscid mesh system (middle), and the boundary layer flow for the shock region (bottom). The shock profile region has been shaded.

Thus in the unsteady inviscid flow, assume that the x-sweeps at the new time have been accomplished as well as the subsequent y-sweeps through the column labeled 0. The boundary layer has been also determined to station 0. We now consider the determination of the flow at station 1, coupling directly the inviscid and boundary layer flows.

From the boundary layer difference equations, an algebraic relation between the velocity U_e (or the pressure) and $d\delta^*/dx$ at the station 1 is obtained in terms of the known conditions at station 0. This relation is

now to apply as the boundary condition at the mesh point 1 for the inviscid flow. Since the pressure is proportional to φ_x in the low frequency limit, the prescribed φ_x along the airfoil ($y = 0$) can be integrated to yield φ at the station 1 in terms of φ at the stations 0 and 1 to second order accuracy. Thus the boundary layer equations yield a boundary condition of the type $\varphi + a\varphi_y = b$ for the inviscid flow; that is a condition of the third type.

In an actual calculation a smaller Δx would be required than shown in Figure 12 for the boundary layer calculations within the shock profile as well as also for the inviscid flow to effect the direct coupling. Thus one undesirability of Le Balleur's procedure for the unsteady problem, namely the need of a fine mesh about the shock profile, is not yet avoided. To remedy this, as well as to seek a more rational and less vulnerable procedure through the shock profile, an ad hoc procedure is suggested for the shock profile region.

It may be recalled that in the case of inviscid flow, the shock profile region was excluded from the physical domain. Thus a fine mesh was used about the shock to minimize this loss of the flow domain. Also, a conservative difference algorithm, insuring a telescoping of the truncation errors, was used to insure the correct jump condition across corresponding points of the excluded region.

The boundary layer underlying the shock profile will be correspondingly treated in a consistent manner, the goal to obtain bridging conditions across the questionable region under the shock profile. Such a bridging condition would relate the boundary layer conditions just downstream of the shock to the known state just upstream of the shock.

Thus consider again Figure 12. Based upon the pressure distribution at the prior time (top of Figure 12), the pre-shock and post-shock points are defined relative to the shock profile. At the downstream station the

43

pressure is assumed to be the empirically observed value as a function of M_1, the Mach number at the upstream station, as used in the viscous ramp procedure. The shock polar is then utilized to obtain the corresponding wedge angle, for example the shock detachment value. The $d\delta^*/dx$ is then assumed to vary in a prescribed manner between this value and the known value at the upstream station. (Here some experimentation with the boundary layer code will be required to evolve a distribution of δ^* through the shock profile to achieve the desired post-shock pressure.) With the resulting δ^* prescribed, the well-behaved indirect boundary layer problem (see Reference 25) is solved to yield the pressure distribution through the shock profile as well as the boundary layer conditions at the post-shock station. The determination of the latter constitutes the bridging condition mentioned earlier. The resulting velocity distribution converted to a potential distribution is then used as a boundary condition for the inviscid flow y-sweeps through the shock profile.

The continuation of the y-sweeps downstream of the shock is treated in the coupled manner described earlier obtaining the starting condition for the boundary layer from the bridging condition.

Here to forestall possible instabilities far downstream, it may be necessary to replace the viscous equations by patching on a suitable asymptotic similarity wake at a sufficiently large distance (perhaps two chords) downstream of the trailing edge. Further, the displacement thickness of such an asymptotic wake may not decrease rapidly enough to be compatible with the freestream conditions prescribed at the downstream computational boundary. A distortion of the asymptotic wake somewhat upstream of the downstream boundary would then be required such that $d\delta^*/dx = 0$ over perhaps a distance of one chord upstream of the boundary. These alterations of the wake occur sufficiently far downstream that they should have little effect on the surface pressure distributions.

In the above procedure, in bridging the shock profile, the $d\delta^*/dx$ obtained from the inviscid flow will not in general agree with the assumed distribution used for the boundary layer. This mismatch might be eliminated by an iterative procedure, but this is probably not warranted due to the questionable validity of the boundary layer equations which assumed a constancy of the pressure across the boundary layer as well as by the use of a vulnerable turbulent entrainment. The inviscid flow is also inadequately treated in this region as mentioned earlier.

The procedure as described above will not require a refined mesh about the shock in the inviscid flow nor iterations at each time step. The procedure described above is a reasonable approach, but its viability must await numerical verification and possible further development. Its formulation has served as a vehicle to focus upon the nature of the difficulties inherent in the problem.

SECTION VI
SUMMARY REMARKS

It is essential that the unsteady fluid dynamic code for use in important aeroelastic problems of swept wings be capable of capturing the important unsteady shock waves. To accomplish this, the appropriate equation in proper conservation form must be used, and the significant viscous interactions at the shock and in the aft region of the wing must be incorporated. It is desirable to incorporate the viscous effects with minimum additional complexity.

Thus time-linearized approximation to the flow equation will be inadequate for important supercritical flows.

Following the steady state developments, second order sweep terms have been added to the classical 3D small disturbance potential equation to insure the correct shock jump conditions. Such an equation does not admit similarity solutions.

For near term application, a viscous ramp procedure is suggested wherein the viscous effects are phenomenologically represented by unsteady shape changes that can then be handled by an inviscid procedure. On a longer time frame a more sophisticated lag entrainment integral method is suggested. In the incorporation of the viscous effects, the 3D flow is first assumed to be quasi-planar in a suitable swept framework; and in the latter, the viscous flow is assumed to be quasi-steady with respect to the instantaneous inviscid flow.

The coupling of the lag entrainment method with the transonic inviscid procedure will be a challenge, particularly if there is a stringent limitation on the added computer time.

46

Finally, one must not forget the resonant wind tunnel wall interference that can have a major effect on aeroelastic phenomena. Its absence must be assured before test data can be validated. The solution to the problem formulated herein will play a vital role for this purpose.

REFERENCES

1. Lomax, H., Bailey, R., and Ballhaus, W., "On the Numerical Simulation of Three-Dimensional Transonic Flow with Application to the C-141", NASA TN-D-6933, 1973.

2. van der Vooren, J., Slooff, J., Huizing, G., and van Essen, A., "Remarks on the Suitability of Various Transonic Small Perturbation Equations to Describe Three-Dimensional Transonic Flow", Proc. Symposium Transsonicum II, 1975.

3. Guderley, G., The Theory of Transonic Flow, Pergamon Press, 1962.

4. Garrick, E., Nonsteady Wing Characteristics, Aerodynamic Components of Aircraft at High Speeds, Vol. VII, Princeton University Press, 1957, pp. 659-667.

5. Ehlers, E., "The Derivation of the Transonic Small Disturbance Differential Equations for the Flow Over Oscillating Three-Dimensional Wings", Boeing Report BCS AM-74, 1978.

6. Courant, R., and Friedrichs, K., Supersonic Flow and Shock Waves, Interscience Publishers, 1948, pp. 121-138.

7. Ballhaus, W., and Bailey, R., "Numerical Calculation of Transonic Flow about Swept Wings", AIAA Paper 72-677, 1972.

8. Schmidt, W., Rohlfs, R., and Vanino, R., "Some Results Using Relaxation Methods for Two and Three-Dimensional Transonic Flows", Presented at the Fourth International Conference on Numerical Methods in Fluid Dynamics, Boulder, Colorado, 1974. (See also Dornier Report FB 74/43, 1974.)

9. Ballhaus, W., Magnus, R., and Yoshihara, H., "Some Examples of Unsteady Transonic Flows over Airfoils", Convair Report CASD-NSC-75-005, 1975.

10. Barnwell, R., "Design and Performance Evaluation of Slotted Walls for Two-Dimensional Wind Tunnels", NASA TM 78648, 1978.

11. Mokry, M., Peake, D., and Bowker, A., "Wall Interference on Two-Dimensional Supercritical Airfoils, using Wall Pressure Measurements to Determine the Porosity Factors for Tunnel Floor and Ceiling", NRC Aero Report LR-575, 1974.

12. Yoshihara, H., and Magnus, R., "Wind Tunnel Wall Interference in Recent High Reynolds Number Transonic Tests on Two-Dimensional Supercritical Airfoils", Convair Report GDC-ERR-73-011, 1973.

13. Pindzola, M., and Lo, C., "Boundary Interference at Subsonic Speeds in Wind Tunnels with Ventilated Walls", AEDC TR-69-47, 1969.

14. Runyan, H., Woolston, D., and Rainey, G., "Theoretical and Experimental Investigation of the Effects of Tunnel Walls on the Forces on an Oscillating Airfoil in Two-Dimensional Subsonic Compressible Flow", NACA TR 1262, 1956.

15. Yoshihara, H., "Fixes to the 3D Transonic Small Disturbance Theory", Convair Report CASD-ERR-75-012, 1975.

16. Riegels, F., and Wittich, H., "Zur Berechnung der Druckverteilung von Profilen", AVA Göttingen Report 41/1/15, 1942.

17. Magnus, R., and Yoshihara, H., "The Transonic Oscillating Flap", AIAA Paper 76-327, 1976.

18. Ghose, S., and Klein, S., "Prediction of Transitory Stall in Two-Dimensional Diffusers", Stanford University Report MD-36, 1976.

19. Green, J., Weeks, D., and Brooman, J., "Prediction of Turbulent Boundary Layers and Wakes in Incompressible Flow by a Lag-Entrainment Method", RAE TR 72231, 1973.

20. Elsenaar, A., van den Berg, B., and Lindhout, J., "Three-Dimensional Separation of an Incompressible Turbulent Boundary Layer on an Infinite Swept Wing", AGARD CP-168, 1975.

21. McLean, D., "Three-Dimensional Turbulent Boundary Layer Calculations for Swept Wings", AIAA Paper 77-3, 1977.

22. Nash, J., and Tseng, R., "The Three-Dimensional Turbulent Boundary Layer on an Infinite Yawed Wing", The Aeronautical Quarterly, November 1971.

23. Mason, W., Mackenzie, D., Stern, M., Ballhaus, W., and Frick, J., "An Automated Procedure for Computing the Three-Dimensional Transonic Flow over Wing-Body Combinations, Including Viscous Effects", AFFDL Report 77-xxxx, 1977.

24. Pearcey, H., Osborn, J., and Haines, B., "The Interaction Between Local Effects at the Shock and Rear Separation", AGARD CP 35, 1968.

25. East, L., Smith, P., and Merryman, P., "Prediction of the Development of Separated Turbulent Boundary Layers by the Lag-Entrainment Method", RAE Report 77046, 1977.

26. Bradshaw, P., Ferriss, D., and Atwell, N., "Calculation of Turbulent Boundary-Layer Development using the Turbulent Energy Equation", J. of Fluid Mech., Vol. 28, 1967, pp. 593-616.

27. Sun, C., and Childs, M., "Wall-Wake Velocity Profile for Compressible Nonadiabatic Flows", AIAA Journal, Vol. 14, No. 6, 1976.

28. Seddon, J., "The Flow Produced by Interaction of a Turbulent Boundary Layer with a Normal Shock of Sufficient Strength to cause Separation", British ARC R&M 3502, 1960.

29. Head, M., "Entrainment in the Turbulent Boundary Layer", British ARC R&M 3152, 1958.

30. Le Balleur, J., Calculs Couplés Visqueux-Non Visqueux incluant Décollements et Ondes de Choc en Écoulement Bidimensionnel, AGARD-LS-94, 1978.

31. Ballhaus, W., and Goorjian, P., "Efficient Solution of Unsteady Transonic Flows about Airfoils", AGARD-CP-226, 1977.

The problem as formulated in Section III, is now derived in more detail and in several representations.

1.0 PHYSICAL, DIMENSIONAL RECTANGULAR COORDINATES AND THE FULL POTENTIAL

1.1 Coordinates and Variables

X,Y,Z	cartesian coordinates with X in the freestream direction and Y in the "spanwise" direction (ft)
T	time (sec)
Φ	velocity potential (ft^2/sec)
P	pressure (lb/ft^2)
ρ	density (slug/ft^3)
γ	ratio of specific heats
a_∞	freestream speed of sound
U_∞	freestream velocity (ft/sec)
P_∞	freestream pressure (lb/ft^2)
ρ_∞	freestream density (slugs/ft^3)

1.2 Pressure Relation

$$\frac{P}{P_\infty} = \left(\frac{\rho}{\rho_\infty}\right)^\gamma$$

$$\frac{\rho}{\rho_\infty} = \left[1 - \frac{(\gamma-1)}{a_\infty^2}\left\{\Phi_T + \frac{1}{2}(\Phi_X^2 + \Phi_Y^2 + \Phi_Z^2 - U_\infty^2)\right\}\right]^{\frac{1}{\gamma-1}}$$

1.3 Flow Differential Equation

$$(\rho)_T + (\rho\Phi_X)_X + (\rho\Phi_Y)_Y + (\rho\Phi_Z)_Z = 0$$

Subscripts denote partial differentiation, and ρ is given in Section 1.2.

1.4 Shock Jump Conditions

Equation of the shock surface: $S(X,Y,Z,T) = X - S^o(Y,Z,T) = 0$

Normal vector to shock surface: $\bar{N}_s = (\bar{H}\,S_T + \bar{I}\,S_X + \bar{J}\,S_Y + \bar{K}\,S_Z)|\bar{N}_s|^{-1}$

$$|\bar{N}_s|^2 = S_T^2 + S_X^2 + S_Y^2 + S_Z^2$$

$\bar{H}, \bar{I}, \bar{J}, \bar{K}$ are unit vectors in T,X,Y,Z directions respectively

Shock velocity (U_s, V_s, W_s) (ft/sec):

$$S_T + S_X U_s + S_Y V_s + S_Z W_s = 0$$

Jump conditions:

$$[\bar{M} \cdot \bar{N}_s] = 0 \qquad \bar{M} = \bar{H}\begin{Bmatrix} \rho \\ \Phi_X \\ \Phi_Y \\ \Phi_Z \end{Bmatrix} + \bar{I}\begin{Bmatrix} \rho\Phi_X \\ -\Phi_T \\ 0 \\ 0 \end{Bmatrix} + \bar{J}\begin{Bmatrix} \rho\Phi_Y \\ 0 \\ -\Phi_T \\ 0 \end{Bmatrix} + \bar{K}\begin{Bmatrix} \rho\Phi_Z \\ 0 \\ 0 \\ -\Phi_T \end{Bmatrix}$$

(In terms of $S^o = X - S(Y, Z, T)$, in the above equations set $S_X = 1$, $S_Y^o = -S_Y$, $S_Z^o = -S_Z$, $S_T^o = -S_T$)

1.5 Wing Boundary Conditions

Equation of wing surface: $B(X,Y,Z,T) = Z - B^o(X,Y,T) = 0$

Wing Tangency Condition:

$$B_T + \Phi_X B_X + \Phi_Y B_Y + \Phi_Z B_Z = 0$$

or

$$B_T^o + \Phi_X B_X^o + \Phi_Y B_Y^o - \Phi_Z = 0$$

Wing Kutta Condition:

$$P^+(X_{TE}, Y, B^o, T) = P^-(X_{TE}, Y, B^o, T)$$

(+ = upper surface; - = lower surface; TE = trailing edge)

1.6 Wake Condition

Equation of Wake: $\qquad W(X,Y,Z,T) = 0$

No Load Condition: $\qquad [P] = P^+ - P^- = 0 \qquad\qquad [-] = \text{jump}$

Flow Tangency Condition: $(\nabla\phi^+ - \nabla\phi^-) \cdot \bar{N}_w = 0$

where $\pm$ denotes the upper or lower surface of the trailing wake and $\bar{N}_w$ is the normal vector of the wake surface $(\bar{N}_w \sim \bar{H}W_T + \bar{I}W_X + \bar{J}W_Y + \bar{K}W_Z)$.

The primary difficulty encountered here is that the side edges of the wake roll up in an ever-tightening "spiral" in the downstream direction making it difficult to fulfill the wake conditions at downstream points. Moreover the potential approximation here ceases to be valid as diffusive effects enter the picture in the tightening "spiral". Here either a "solid core" must be introduced or more drastically the wake condition must be imposed in a quasi-planar fashion. Such downstream oversimplified modeling, fortunately does not significantly distort the flow over the wing.

1.7 Outer Conditions (Approximate)

Far upstream boundary: $\qquad \phi = U_\infty X$

Far lateral boundaries:

$$\phi_n = 0 \text{ (Solid walls)}$$

Far downstream boundary (Quasi-planar wake)

$$\phi_T + U_\infty(\phi_X - U_\infty) = 0$$

54

1.8 Wind Tunnel Wall Conditions (Highly Idealized)

On side walls:

$$\frac{P - P_\infty}{\frac{1}{2}\rho_\infty U_\infty^2} + K_o \Phi_{XY} + \frac{1}{R_o}\Phi_Y = 0$$

On upper or lower walls:

$$\frac{P - P_\infty}{\frac{1}{2}\rho_\infty U_\infty^2} + K_o \Phi_{XZ} + \frac{1}{R_o}\Phi_Z = 0$$

$$R_o \to 0: \text{ solid wall}$$
$$R_o \to \infty, K_o = 0: \text{ free jet}$$
$$R_o \to \infty: \text{ slotted wall}$$
$$K_o = 0: \text{ perforated wall}$$

2.0 PHYSICAL, NON-DIMENSIONAL RECTANGULAR COORDINATES AND THE DISTURBANCE POTENTIAL

2.1 Coordinates and Variables

$$x = X/c \qquad y = Y/c \qquad z = Z/c$$

$$t = (U_\infty/c)\, T$$

$$\varphi(x,y,z,t) = \Phi(X,Y,Z,T)/(U_\infty c) - x$$

(all lower case variables are non-dimensional and c is a reference chord.)

2.2 Pressure Relation (through second order in φ)

$$C_p = \frac{P - P_\infty}{\frac{1}{2}\rho_\infty U_\infty^2} = -2(\varphi_x + \varphi_t) - \left\{ (1 - M_\infty^2)\varphi_x^2 + \varphi_y^2 + \varphi_z^2 \right.$$

$$\left. - M_\infty^2(\varphi_t^2 + 2\varphi_x\varphi_t) \right\} + \cdots$$

55

2.3 Differential Equation (To Second Order)

$$(f_o)_t + (f_1)_x + (f_2)_y + (f_3)_z = 0$$

where

$$f_o = -M_\infty^2 (\varphi_x + 2\varphi_t) + \frac{1}{2} M_\infty^2 \left\{ 1-(2-\gamma)M_\infty^2 \right\} \varphi_x^2$$

$$+ \frac{1}{2} M_\infty^2 (\varphi_y^2 + \varphi_z^2) + \frac{1}{2}(2-\gamma)M_\infty^4 (\varphi_t^2 + 2\varphi_x \varphi_t) + \cdots$$

$$f_1 = (1- M_\infty^2)\varphi_x - \frac{1}{2}(\gamma+1) M_\infty^2 \left\{ 1-\left(\frac{\gamma-2}{\gamma+1}\right)(1-M_\infty^2) \right\} \varphi_x^2 - \frac{1}{2}M_\infty^2 (\varphi_y^2 + \varphi_z^2)$$

$$+ \frac{1}{2}(2-\gamma)M_\infty^4 \varphi_t^2 - M_\infty^4 \left\{ 1-(2-\gamma)M_\infty^2 \right\} \varphi_x \varphi_t + \cdots$$

$$f_2 = \left\{ 1- M_\infty^2(\varphi_x + \varphi_t) \right\} \varphi_y$$

$$f_3 = \left\{ 1- M_\infty^2(\varphi_x + \varphi_t) \right\} \varphi_z .$$

2.4 Shock Jump Conditions (To Second Order)

Equation of shock surface: $\qquad S(x,y,z,t) = x - S^o(y,z,t) = 0$

Shock jump conditions:

$$[f_o] S_t + [f_1] S_x + [f_2] S_y + [f_3] S_z = 0$$

$$[\varphi_x] S_t - [\varphi_t] S_x \qquad\qquad = 0$$

$$[\varphi_y] S_t \qquad - [\varphi_t] S_y \qquad = 0$$

$$[\varphi_z] S_t \qquad\qquad - [\varphi_t] S_z = 0$$

Shock velocity (u_s, v_s, w_s):

$$S_t + u_s S_x + v_s S_y + w_s S_z = 0$$

Here $u_s = U_s/U_\infty$, etc..

56

2.5 Wing Boundary Condition (To First Order)

Equation of wing:
$$z - \overset{\circ}{b}(x,y,t) = 0$$

Tangency condition:

$$b_t^\circ + b_x^\circ - \varphi_z(x,y,0^\pm,t) = 0$$

Kutta condition:

$$\varphi_x(x_{TE}, y, 0^+, t) + \varphi_t(x_{TE}, y, 0^+, t) =$$

$$\varphi_x(x_{TE}, y, 0^-, t) + \varphi_t(x_{TE}, y, 0^-, t).$$

(0^+ = upper surface; 0^- = lower surface; TE = trailing edge).

2.6 Wake Condition (Planar, First Order)

No load condition:
$$\varphi_x(x,y,0^+,t) + \varphi_t(x,y,0^+,t)$$

$$= \varphi_x(x,y,0^-,t) + \varphi_t(x,y,0^-,t)$$

Tangency condition:

$$\varphi_z(x,y,0^+,t) = \varphi_z(x,y,0^-,t)$$

57

2.7 Outer Conditions

Far upstream boundary: $\varphi = 0$

Far lateral boundaries:

$$\varphi_n = 0$$

Far downstream boundary:

$$\varphi_x + \varphi_t = 0$$

2.8 Wind Tunnel Wall Conditions $\left(K = U_\infty c \, K_o \; ; \; \frac{1}{R} = U_\infty c \frac{1}{R_o} \right)$

Side walls: $-2(\varphi_x + \varphi_t) + K \varphi_{xy} + \frac{1}{R} \varphi_y = 0$

Upper or lower walls:

$$-2(\varphi_x + \varphi_t) + K \varphi_{xz} + \frac{1}{R} \varphi_z = 0$$

3.0 SCALED, NON-DIMENSIONAL RECTANGULAR COORDINATES AND THE DISTURBANCE POTENTIAL.

3.1 Scaling

$$X = \tilde{x} \qquad y = \tilde{y}/\nu \qquad z = \tilde{z}/\mu$$

$$t = \tilde{t}/\tau$$

$$\varphi(x, y, z, t) = \epsilon \, \tilde{\varphi}(\tilde{x}, \tilde{y}, \tilde{z}, \tilde{t})$$

58

3.2 Pressure Relation

$$C_p = -2\epsilon(\tilde{\varphi}_{\tilde{x}} + \tau\,\tilde{\varphi}_{\tilde{t}}) - \epsilon^2\left\{(1-M_\infty^2)\,\tilde{\varphi}_{\tilde{x}}^{\,2} + \nu^2\tilde{\varphi}_{\tilde{y}}^{\,2} + \mu^2\tilde{\varphi}_{\tilde{z}}^{\,2}\right\} + \cdots$$

3.3 Differential Equation

$$(\tilde{f}_0)_{\tilde{t}} + (\tilde{f}_1)_{\tilde{x}} + (\tilde{f}_2)_{\tilde{y}} + (\tilde{f}_3)_{\tilde{z}} = 0$$

$$\tilde{f}_0 = -\epsilon\tau M_\infty^2(\tilde{\varphi}_{\tilde{x}} + 2\tau\tilde{\varphi}_{\tilde{t}}) - \tfrac{1}{2}\epsilon^2\tau M_\infty^2\left[-(2-\gamma)M_\infty^2(\tau^2\tilde{\varphi}_{\tilde{t}}^{\,2} + 2\tau\,\tilde{\varphi}_{\tilde{x}}\,\tilde{\varphi}_{\tilde{t}})\right.$$

$$\left. + \left\{1-(2-\gamma)M_\infty^2\right\}\tilde{\varphi}_{\tilde{x}}^{\,2} + \nu^2\tilde{\varphi}_{\tilde{y}}^{\,2} + \mu^2\tilde{\varphi}_{\tilde{z}}^{\,2}\right] + \cdots$$

$$\tilde{f}_1 = \epsilon(1-M_\infty^2)\tilde{\varphi}_{\tilde{x}} - \tfrac{1}{2}\epsilon^2 M_\infty^2\left[-(2-\gamma)\tau^2 M_\infty^2\,\tilde{\varphi}_{\tilde{t}}^{\,2}\right.$$

$$+ 2\tau\left\{1-(2-\gamma)M_\infty^2\right\}\tilde{\varphi}_{\tilde{x}}\,\tilde{\varphi}_{\tilde{t}}$$

$$+ (\gamma+1)\left\{1-\left(\frac{\gamma-2}{\gamma+1}\right)(1-M_\infty^2)\right\}\tilde{\varphi}_{\tilde{x}}^{\,2}$$

$$\left. + \nu^2\tilde{\varphi}_{\tilde{y}}^{\,2} + \mu^2\tilde{\varphi}_{\tilde{z}}^{\,2}\right] + \cdots$$

$$\tilde{f}_2 = \epsilon\nu^2\left\{1-\epsilon M_\infty^2(\tilde{\varphi}_{\tilde{x}} + \tau\,\tilde{\varphi}_{\tilde{t}})\right\}\tilde{\varphi}_{\tilde{y}} + \cdots$$

$$\tilde{f}_3 = \epsilon\mu^2\left\{1-\epsilon M_\infty^2(\tilde{\varphi}_{\tilde{x}} + \tau\,\tilde{\varphi}_{\tilde{t}})\right\}\tilde{\varphi}_{\tilde{z}} + \cdots.$$

3.4 Shock Jump Conditions

Equation of shock surface: $\tilde{S}(\tilde{x}, \tilde{y}, \tilde{z}, \tilde{t}) = 0$

Jump conditions:

$$[\tilde{f}_o]\,\tilde{S}_{\tilde{t}} + [\tilde{f}_1]\,\tilde{S}_{\tilde{x}} + [\tilde{f}_2]\,\tilde{S}_{\tilde{y}} + [\tilde{f}_3]\,\tilde{S}_{\tilde{z}} = 0$$

$$[\tilde{\varphi}_{\tilde{y}}]\,\tilde{S}_{\tilde{t}} - [\tilde{\varphi}_{\tilde{t}}]\,\tilde{S}_{\tilde{x}} \qquad\qquad = 0$$

$$[\tilde{\varphi}_{\tilde{y}}]\,\tilde{S}_{\tilde{t}} \qquad\quad - [\tilde{\varphi}_{\tilde{t}}]\,\tilde{S}_{\tilde{y}} \qquad = 0$$

$$[\tilde{\varphi}_{\tilde{z}}]\,\tilde{S}_{\tilde{t}} \qquad\qquad\quad - [\tilde{\varphi}_{\tilde{t}}]\,\tilde{S}_{\tilde{z}} = 0 .$$

Shock velocity

$$\tilde{S}_{\tilde{t}} + \tilde{u}_s\,\tilde{S}_{\tilde{x}} + \tilde{v}_s\,\tilde{S}_{\tilde{y}} + \tilde{w}_s\,\tilde{S}_{\tilde{z}} = 0$$

$$\tilde{u}_s = \left.\frac{d\tilde{x}}{d\tilde{t}}\right|_{\tilde{S}=0} = \frac{1}{\tau}\,u_s \;\; ; \quad \tilde{v}_s = \frac{\nu}{\tau}\,v_s \;\; ; \quad \tilde{w}_s = \frac{\mu}{\tau}\,w_s .$$

3.5 Wing Boundary Condition

Equation of wing: $\tilde{z} - \mu\delta\,\tilde{b}^o(\tilde{x}, \tilde{y}, \tilde{t}) = 0$

Tangency condition:
$$\tilde{\varphi}_{\tilde{z}} = \frac{\delta}{\epsilon\mu}\,(\tilde{b}^o_{\tilde{x}} + \tau\,\tilde{b}^o_t)$$

Kutta condition:

$$\tilde{\varphi}_{\tilde{x}}(\tilde{x}_{TE}, \tilde{y}, 0^+, \tilde{t}) + \tau\,\tilde{\varphi}_{\tilde{t}}(\tilde{x}_{TE}, \tilde{y}, 0^+, \tilde{t})$$

$$= \tilde{\varphi}_{\tilde{x}}(\tilde{x}_{TE}, \tilde{y}, 0^-, \tilde{t}) + \tau\,\tilde{\varphi}_{\tilde{t}}(\tilde{x}_{TE}, \tilde{y}, 0^-, \tilde{t}) .$$

60

3.6 Wake Condition

No load condition:

$$\tilde{\varphi}_{\tilde{x}}(\tilde{x},\tilde{y},0^+,\tilde{t}) + \tau\,\tilde{\varphi}_{\tilde{t}}(\tilde{x},\tilde{y},0^+,\tilde{t})$$

$$= \tilde{\varphi}_{\tilde{x}}(\tilde{x},\tilde{y},0^-,\tilde{t}) + \tau\,\tilde{\varphi}_{\tilde{t}}(\tilde{x},\tilde{y},0^-,\tilde{t})$$

Tangency condition:

$$\tilde{\varphi}_{\tilde{z}}(\tilde{x},\tilde{y},0^+,\tilde{t}) = \tilde{\varphi}_{\tilde{z}}(\tilde{x},\tilde{y},0^-,\tilde{t})$$

3.7 Outer Conditions

Far upstream boundary: $\qquad \tilde{\varphi} = 0$

Far lateral boundary:

$$\tilde{\varphi}_n = 0$$

Far downstream boundary:

$$\tilde{\varphi}_{\tilde{x}} + \tau\,\tilde{\varphi}_{\tilde{t}} = 0$$

3.8 Wind Tunnel Wall Conditions

Side walls: $\qquad -2(\tilde{\varphi}_{\tilde{x}} + \tau\tilde{\varphi}_{\tilde{t}}) + K\,\nu\,\tilde{\varphi}_{\tilde{x}\tilde{y}} + \dfrac{1}{R}\,\nu\,\tilde{\varphi}_{\tilde{y}} = 0$

Upper or lower walls:

$$-2(\tilde{\varphi}_{\tilde{x}} + \tau\tilde{\varphi}_{\tilde{t}}) + K\,\mu\,\tilde{\varphi}_{\tilde{x}\tilde{z}} + \frac{1}{R}\,\mu\,\tilde{\varphi}_{\tilde{z}} = 0$$

61

4.0 SPECIAL CASE: TRANSONIC SCALING

4.1 Scaling

$$\nu = \sigma \delta^{\frac{1}{3}} \quad ; \quad \mu = \delta^{\frac{1}{3}} \quad ; \quad \tau = \beta \delta^{\frac{2}{3}}$$

$$\epsilon = \delta^{\frac{2}{3}} \quad ; \quad (1-M_\infty^2) = K \delta^{\frac{2}{3}} \; .$$

4.2 Pressure Relation

$$C_p = -2 \delta^{\frac{2}{3}} \tilde{\varphi}_{\tilde{x}} - 2 \delta^{\frac{4}{3}} \beta \tilde{\varphi}_{\tilde{t}} - \delta^2 \left\{ K \tilde{\varphi}_{\tilde{x}}^2 + \sigma^2 \tilde{\varphi}_{\tilde{y}}^2 + \tilde{\varphi}_{\tilde{z}}^2 \right\} + \cdots$$

4.3 Differential Equation

$$\underline{(\tilde{f}_0)_{\tilde{t}} + (\tilde{f}_1)_{\tilde{x}} + (\tilde{f}_2)_{\tilde{y}} + (\tilde{f}_3)_{\tilde{z}} = 0}$$

$$\tilde{f}_0 = -2\beta \, \delta^{\frac{4}{3}} M_\infty^2 \, \tilde{\varphi}_{\tilde{x}} - \beta \delta^2 M_\infty^2 \left[\beta \tilde{\varphi}_{\tilde{t}} + \frac{1}{2} \left\{ 1-(2-\gamma)M_\infty^2 \right\} \tilde{\varphi}_{\tilde{x}}^2 \right]$$

$$+ \cdots$$

$$\tilde{f}_1 = \delta^{\frac{4}{3}} \left[-K \tilde{\varphi}_{\tilde{x}} - \frac{1}{2} M_\infty^2 (\gamma+1) \tilde{\varphi}_{\tilde{x}}^2 \right]$$

$$+ (2-\gamma) \delta^2 M_\infty^2 \left(\frac{1}{2} K \tilde{\varphi}_{\tilde{x}}^2 + \beta M_\infty^2 \tilde{\varphi}_{\tilde{x}} \tilde{\varphi}_{\tilde{t}} \right)$$

$$- \frac{1}{2} M_\infty^2 \delta^{\frac{8}{3}} \left[\sigma^2 \tilde{\varphi}_{\tilde{y}}^2 + \tilde{\varphi}_{\tilde{z}}^2 - (2-\gamma) \beta^2 M_\infty^2 \tilde{\varphi}_{\tilde{t}}^2 \right] + \cdots$$

$$\tilde{f}_2 = \delta^{\frac{4}{3}} \sigma^2 \tilde{\varphi}_{\tilde{y}} - \sigma^2 \delta^2 M_\infty^2 \tilde{\varphi}_{\tilde{x}} \tilde{\varphi}_{\tilde{y}} - \beta \sigma^2 \delta^{\frac{8}{3}} \tilde{\varphi}_{\tilde{y}} \tilde{\varphi}_{\tilde{t}} + \cdots$$

$$\tilde{f}_3 = \delta^{\frac{4}{3}} \tilde{\varphi}_{\tilde{z}} - \delta^2 M_\infty^2 \tilde{\varphi}_{\tilde{x}} \tilde{\varphi}_{\tilde{z}} - \beta \delta^{\frac{8}{3}} M_\infty^2 \tilde{\varphi}_{\tilde{z}} \tilde{\varphi}_{\tilde{t}} + \cdots \; .$$

4.4 Shock Jump Conditions

Identical to Section 3.4 with $\tilde{f}_0$, $\tilde{f}_1$, $\tilde{f}_2$, $\tilde{f}_3$ obtained from Section 4.3.

4.5 Wing Boundary Condition

Equation of wing:

$$\tilde{z} - \delta^{\frac{4}{3}} \tilde{b}^{\,o}(\tilde{x}, \tilde{y}, \tilde{t}) = 0$$

Tangency condition:

$$\tilde{\varphi}_{\tilde{z}} = \tilde{b}^{\,o}_{\tilde{x}} + \beta \delta^{\frac{2}{3}} \tilde{b}^{\,o}_{\tilde{t}}$$

Kutta condition:

$$\tilde{\varphi}_{\tilde{x}}(\tilde{x}_{TE}, \tilde{y}, 0^+, \tilde{t}) - \tilde{\varphi}_{\tilde{x}}(\tilde{x}_{TE}, \tilde{y}, 0^-, \tilde{t})$$

$$+ \beta \delta^{\frac{2}{3}} \left\{ \tilde{\varphi}_{\tilde{t}}(\tilde{x}_{TE}, \tilde{y}, 0^+, \tilde{t}) - \tilde{\varphi}_{\tilde{t}}(\tilde{x}_{TE}, \tilde{y}, 0^-, \tilde{t}) \right\} = 0$$

4.6 Wake Condition

No load condition:

$$\tilde{\varphi}_{\tilde{x}}(\tilde{x}, \tilde{y}, 0^+, \tilde{t}) - \tilde{\varphi}_{\tilde{x}}(\tilde{x}, \tilde{y}, 0^-, \tilde{t})$$

$$+ \beta \delta^{\frac{2}{3}} \left\{ \tilde{\varphi}_{\tilde{t}}(\tilde{x}, \tilde{y}, 0^+, \tilde{t}) - \tilde{\varphi}_{\tilde{t}}(\tilde{x}, \tilde{y}, 0^-, \tilde{t}) \right\} = 0$$

Tangency condition:

$$\tilde{\varphi}_{\tilde{z}}(\tilde{x}, \tilde{y}, 0^+, \tilde{t}) = \tilde{\varphi}_{\tilde{z}}(\tilde{x}, \tilde{y}, 0^-, \tilde{t})$$

63

4.7 Outer Conditions

Far upstream conditions: $\tilde{\varphi} = 0$

Far lateral condition:

$$\tilde{\varphi}_{\tilde{n}} = 0$$

Far downstream boundary:

$$\tilde{\varphi}_{\tilde{x}} + \beta \delta^{\frac{2}{3}} \tilde{\varphi}_{\tilde{t}} = 0$$

4.8 Wind Tunnel Wall Conditions

Side walls: $\quad -2\tilde{\varphi}_{\tilde{x}} + \sigma\delta^{\frac{1}{3}}(K\,\tilde{\varphi}_{\tilde{x}\tilde{y}} + \frac{1}{R}\,\tilde{\varphi}_{\tilde{y}}) - 2\beta\delta^{\frac{2}{3}}\tilde{\varphi}_{\tilde{t}} = 0$

Upper or low walls:

$$-2\tilde{\varphi}_{\tilde{x}} + \delta^{\frac{1}{3}}(K\,\tilde{\varphi}_{\tilde{x}\tilde{y}} + \frac{1}{R}\,\tilde{\varphi}_{\tilde{z}}) - 2\beta\delta^{\frac{2}{3}}\tilde{\varphi}_{\tilde{z}} = 0$$

4.9 Comments

If in the above equations, we take the limit as $\delta \to 0$, we obtain the low unsteadiness case defined in Section III Subsection 7.0, with the spanwise effects represented only by the φ_{yy} term. There is no scaling of the time to obtain the high unsteadiness case with the φ_{tt} term in this limiting process.

The corresponding limiting shock jump conditions are those labeled Guderley-von Karman in Figure 1; and as seen previously, they are completely inadequate for swept shocks being satisfactory only for shocks essentially normal to the freestream.

If we examine the effect of the transonic scaling on the wing planform shape distortion in the limit $\delta \to 0$, an untapered, unswept wing planform of infinite aspect ratio is obtained, so that the limiting shock jump conditions are not inconsistent with the distorted planform.

It is amply clear that no scaling exists for which a physically meaningful limiting process would yield the basic flow equation, Eq. (4) suitable for swept wings.

64

The basic flow equation (4) will now be transformed in proper conservation form in the sheared coordinate system of Section 3.0. The relevant theory to accomplish this can be found in Lass, "Vector and Tensor Analysis, McGraw-Hill, 1950, specifically in Eqs. (491) and (528).

The starting point is Eq. (4) given by

$$\frac{\partial f_0}{\partial t} + \frac{\partial f_1}{\partial x} + \frac{\partial f_2}{\partial y} + \frac{\partial f_3}{\partial z} = 0$$

where

$$f_0 = -\sigma(\sigma \varphi_t + \varphi_x)$$

$$f_1 = K\varphi_x - B\varphi_x^2 - \sigma\varphi_t - \frac{1}{2}\varphi_y^2 \qquad K = \frac{1-M_\infty^2}{M_\infty^2}$$

$$f_2 = M_\infty^{-2}(1 - M_\infty^2 \varphi_x)\varphi_y \qquad \text{(B1)}$$

$$f_3 = M_\infty^{-2}\varphi_z \qquad B = \frac{1}{2}(\gamma+1)\left\{1 - \left(\frac{\gamma-2}{\gamma+1}\right)(1-M_\infty^2)\right\}$$

The shearing transformation is given by

$$\xi = \frac{x - x_{LE}(y)}{C(y)}$$

$$\eta = y \qquad \tilde{\varphi}(\xi, \eta, \zeta, t) = \varphi(x, y, z, t) \qquad \text{(B2)}$$

$$\zeta = z$$

From Eq. (528) from the above reference, the transformed equation in conservation form is given by

$$\frac{\partial(\sqrt{g}\,\tilde{f}_0)}{\partial t} + \frac{\partial(\sqrt{g}\,\tilde{f}_1)}{\partial \xi} + \frac{\partial(\sqrt{g}\,\tilde{f}_2)}{\partial \eta} + \frac{\partial(\sqrt{g}\,\tilde{f}_3)}{\partial \zeta} = 0 \qquad \text{(B3)}$$

where g is the determinant of the metric tensor of the sheared transformation (B2) and is given by $g = c^2(y)$ (see Lass, p. 279); and $\tilde{f}_0, \tilde{f}_1, \tilde{f}_2, \tilde{f}_3$ are the transformed components of the contravariant mass flux vector given by (see Lass, Eq. 491)

$$\tilde{f}_0 = f_0$$

$$\tilde{f}_1 = \frac{1}{c}f_1 + \xi_y f_2$$

$$\tilde{f}_2 = f_2 \tag{B4}$$

$$\tilde{f}_3 = f_3 \; .$$

where ξy from Eq. (B2) is

$$\xi_y = -\frac{1}{c}(x'_{LE} + \xi c')$$

primes denoting differentiation with respect to y.

Finally in Eq. (B4) we must transform the derivatives arising on the right side with the result

$$\tilde{f}_0 = -\sigma(\sigma\tilde{\varphi}_t + \frac{1}{c}\tilde{\varphi}_\xi)$$

$$\tilde{f}_1 = (\frac{K}{c^2} + M_\infty^{-2}\xi_y^2)\tilde{\varphi}_\xi + M_\infty^{-2}\xi_y\tilde{\varphi}_\eta - \frac{\sigma}{c}\tilde{\varphi}_t - (\frac{3}{2}\frac{1}{c}\xi_y^2 + \frac{B}{c^3})\tilde{\varphi}_\xi^2 - \frac{1}{2c}\tilde{\varphi}_\eta^2 - \frac{2\xi_y}{c}\tilde{\varphi}_\xi\tilde{\varphi}_\eta$$

$$\tilde{f}_2 = M_\infty^{-2}\xi_y\tilde{\varphi}_\xi + M_\infty^{-2}\tilde{\varphi}_\eta - \frac{1}{c}\xi_y\tilde{\varphi}_\xi^2 - \frac{1}{c}\tilde{\varphi}_\xi\tilde{\varphi}_\eta \tag{B5}$$

$$\tilde{f}_3 = M_\infty^{-2}\tilde{\varphi}_\zeta$$

Thus Eq. (B5) together with Eq. (B3) with $\sqrt{g} = c(y)$ constitute the transformed equation in conservation form. It is the proper conservation form with the components given in Eqs. (B4) and (B5) representing components of the mass flux vector.

66
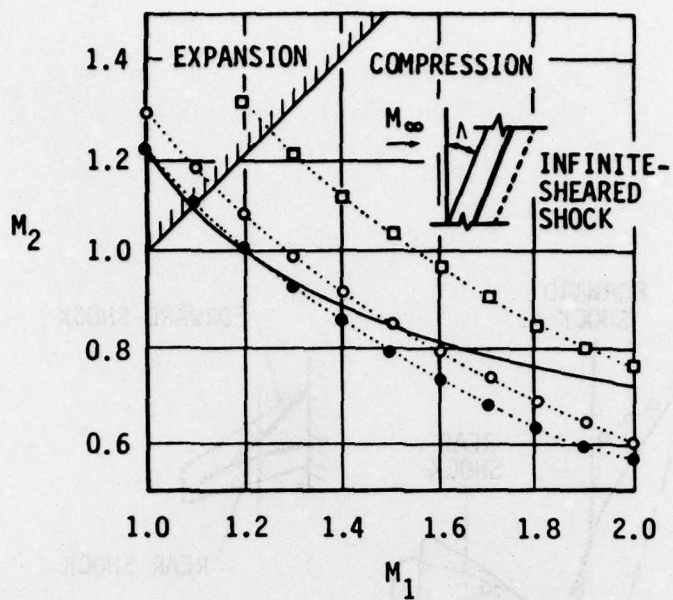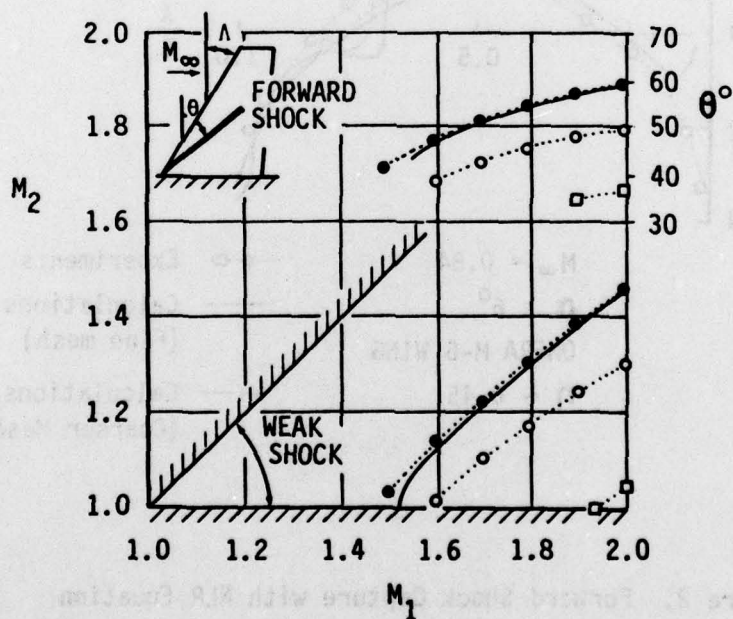
Figure 1. Shock Jump Conditions for Various Equations

67
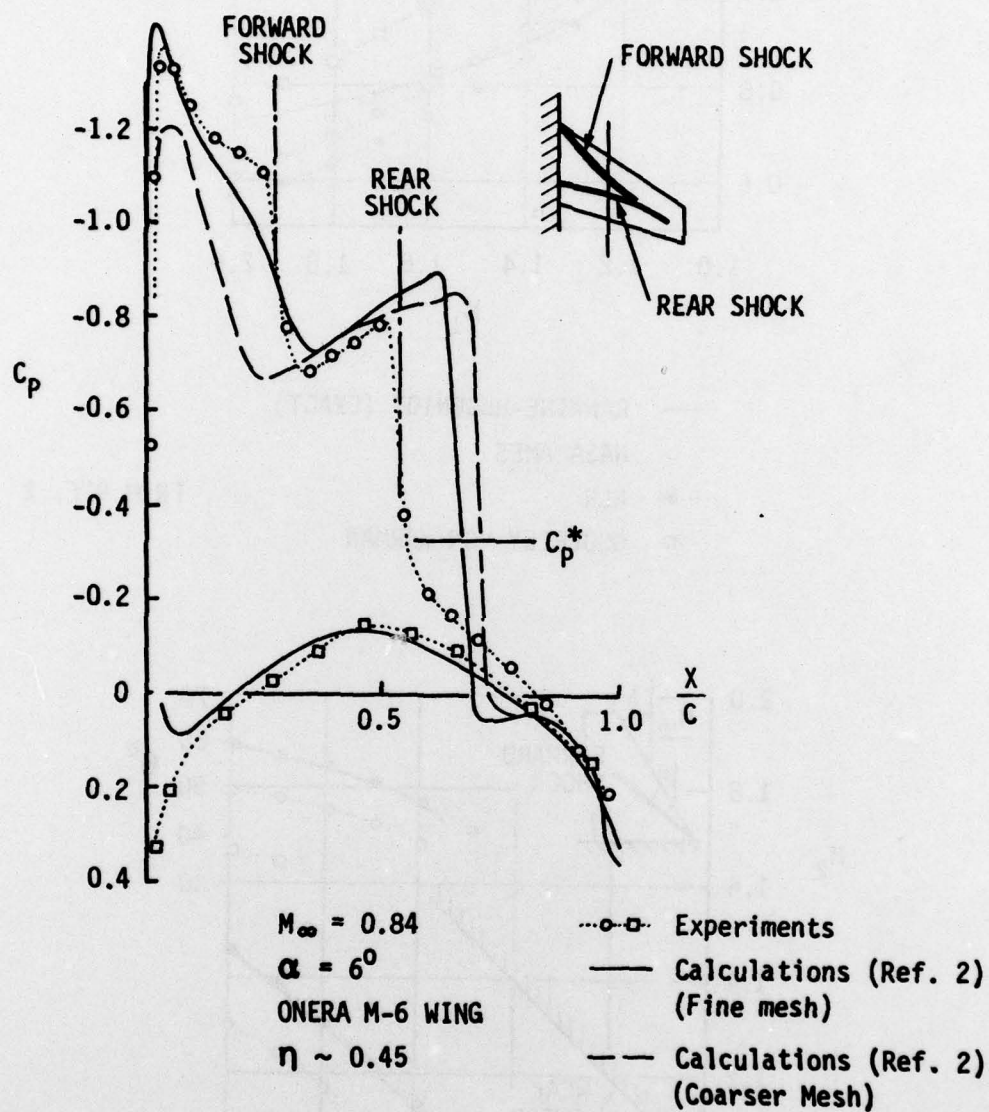
Figure 2. Forward Shock Capture with NLR Equation

68
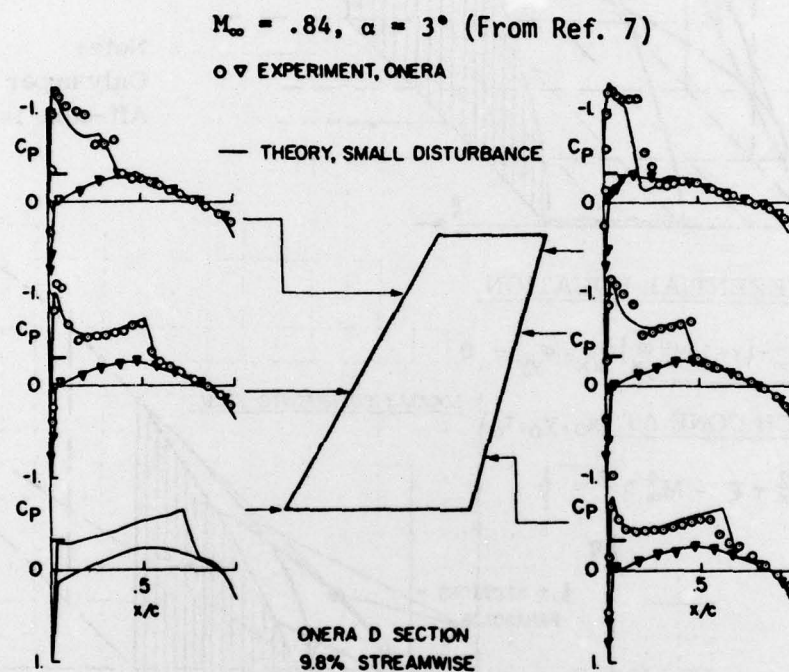
Figure 3. Shock Capture with NASA Equation

LOCALLY SUBSONIC FLOW

η, τ SECTIONS = HYPERBOLAS

ξ, η SECTIONS = PARABOLAS

η

τ

ξ

P

Note:
Only upper half of the
Aft-cone is shown
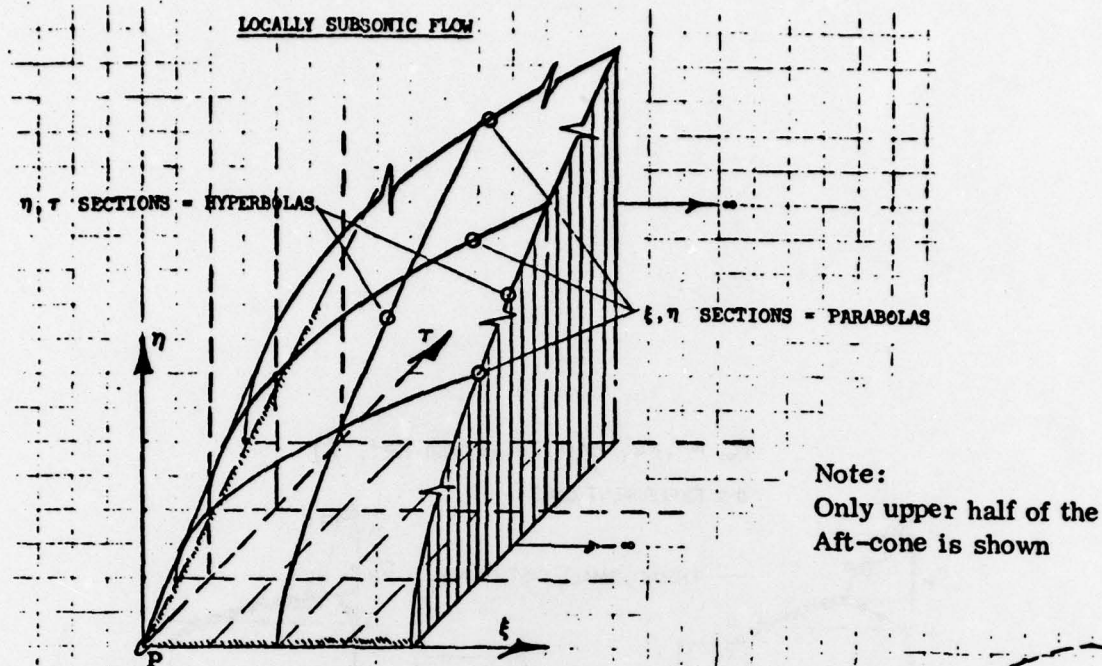
FLOW DIFFERENTIAL EQUATION

$$2M_\infty^2 \varphi_{xt} - [1 - M_\infty^2 - (\gamma+1)M_\infty^2 \varphi_x] \varphi_{xx} - \varphi_{yy} = 0$$

LOCAL MACH CONE AT (x_0, y_0, t_0)

LOCALLY SUPERSONIC FLOW

$$V_c \tau^2 + 2M_\infty^2 \tau \xi - M_\infty^4 \eta^2 = 0$$

$\xi = x - x_0$

$\eta = y - y_0$

$\tau = t - t_0$

ξ, η SECTIONS = PARABOLAS

η

η, τ SECTIONS = ELLIPSES

ξ

P

$-\tau$
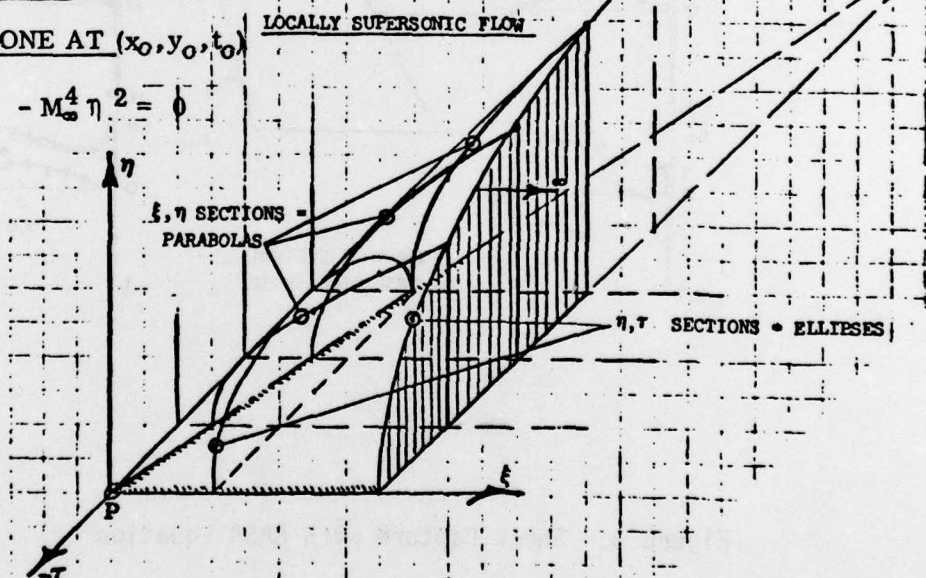
Figure 4.   "Mach Cone" for the 2-D Low Frequency Equation

70
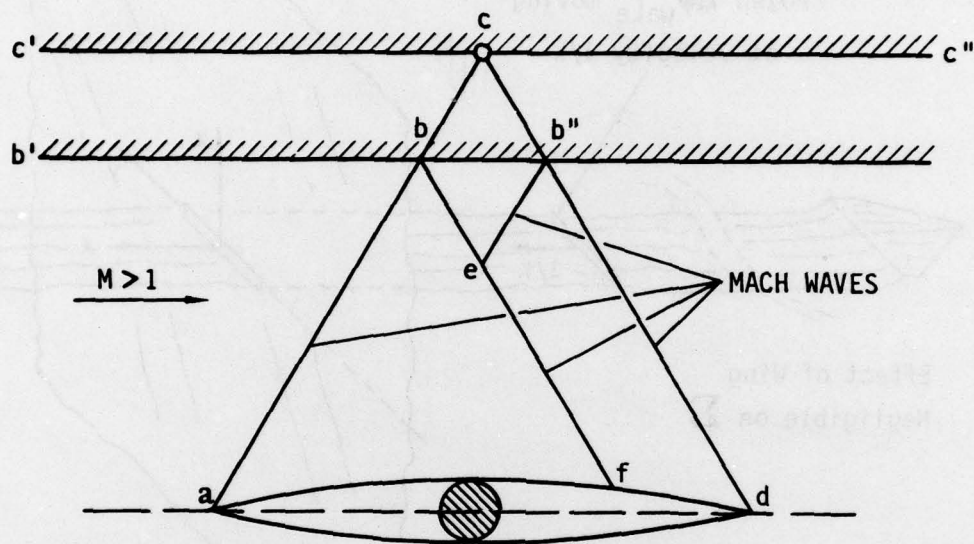
Figure 5. Far-Field Condition - Hyberbolic Case

71

$\sum$ (Far downstream boundary, $x = x_0$)

Frozen $\Delta\phi_{wake}$ moving at velocity 1/k

Effect of Wing Negligible on $\sum$
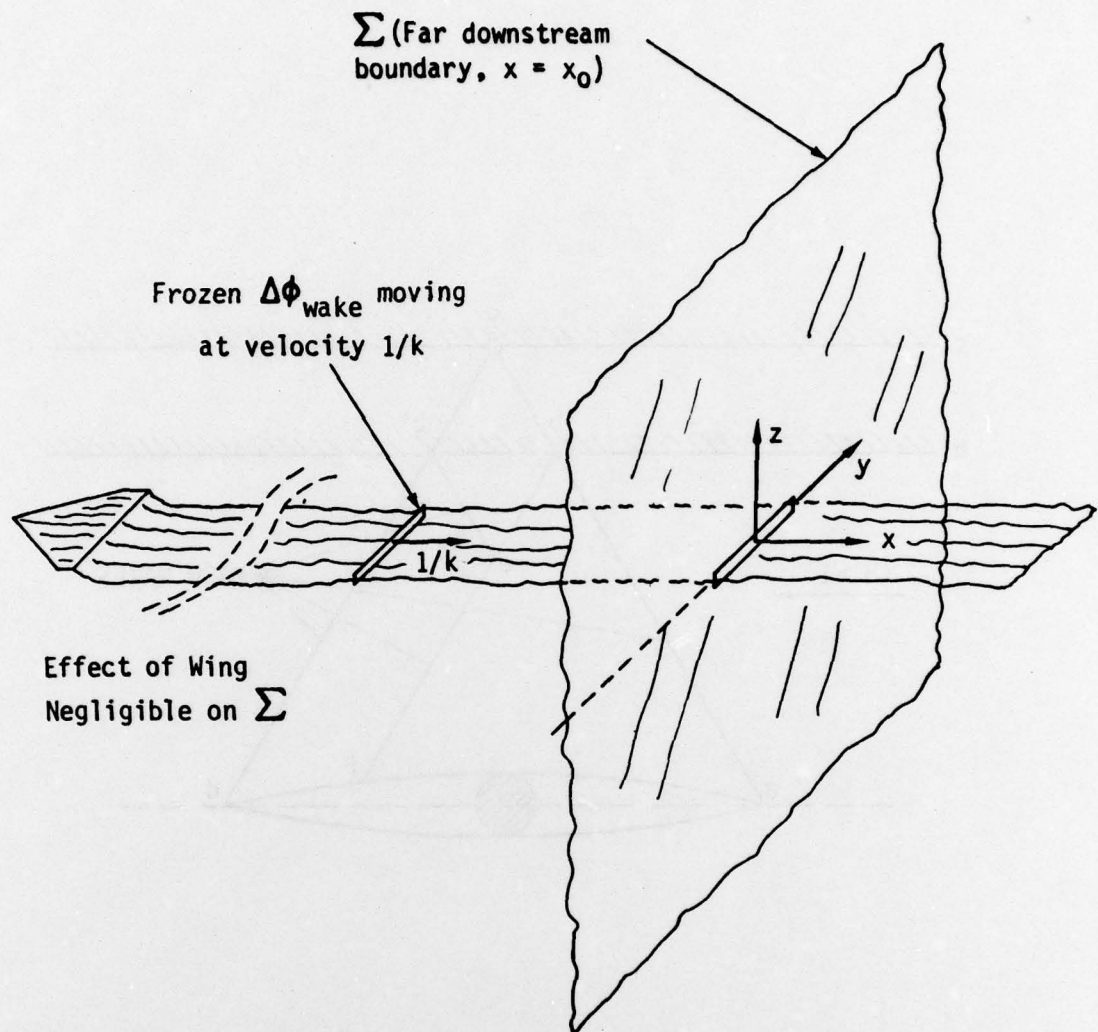
On $\sum$:

$$\phi(x_0, y, t + \Delta t) = \phi(x_0 - 1/k\Delta t, y, t)$$

or $\boxed{k\phi_t + \phi_x = 0}$

Figure 6. Far Downstream Boundary Condition (Trefftz Plane)

72
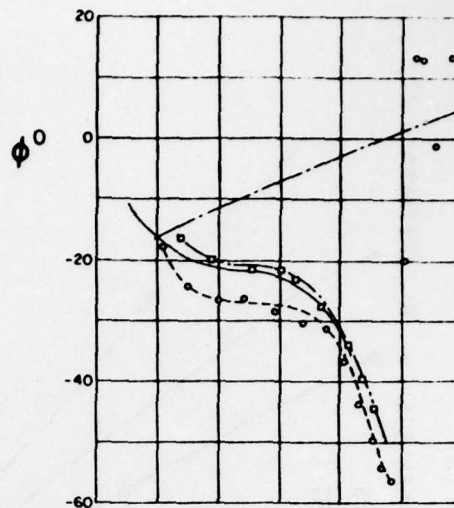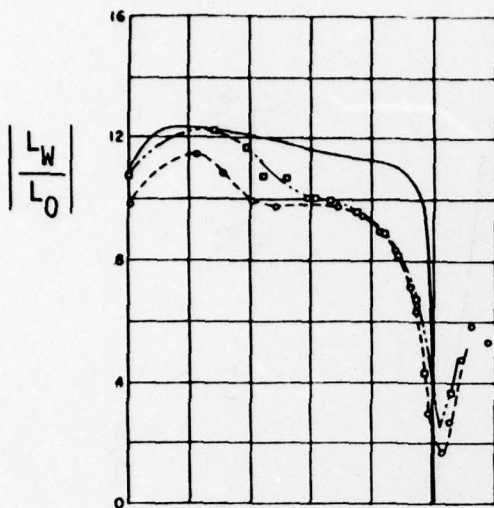
$|L_W|$ Lift Amplitude with Walls

$|L_0|$ Lift Amplitude without Walls

$|M_W|$ Pitching Moment Amplitude with Walls

$|M_0|$ Pitching Moment Amplitude without Walls

ϕ^0 Phase Angle between L or M and the Airfoil Motion

---o--- Test M = 0.67

---□--- Test M = 0.71 (From Ref. 14)

——— Theory with Walls M = 0.7

—·— Theory without Walls M = 0.7
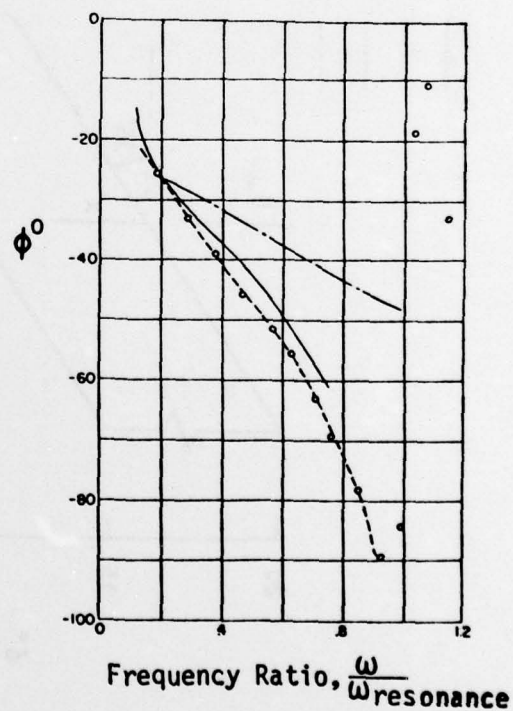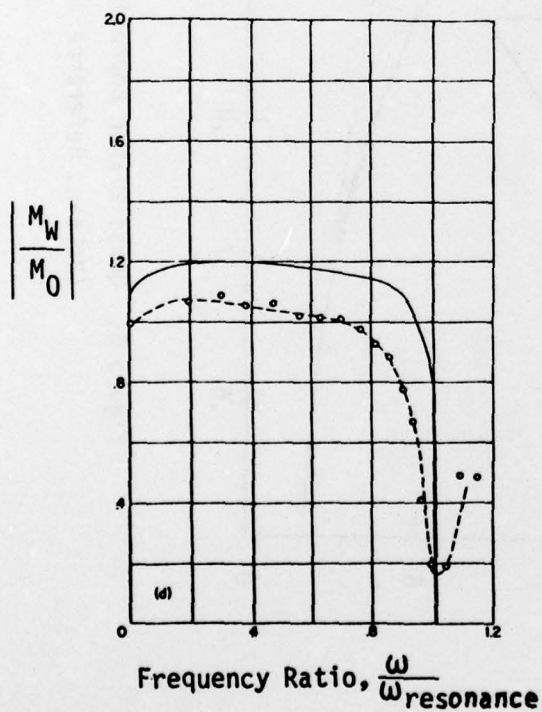
Figure 7. Resonant Wall Interference

73
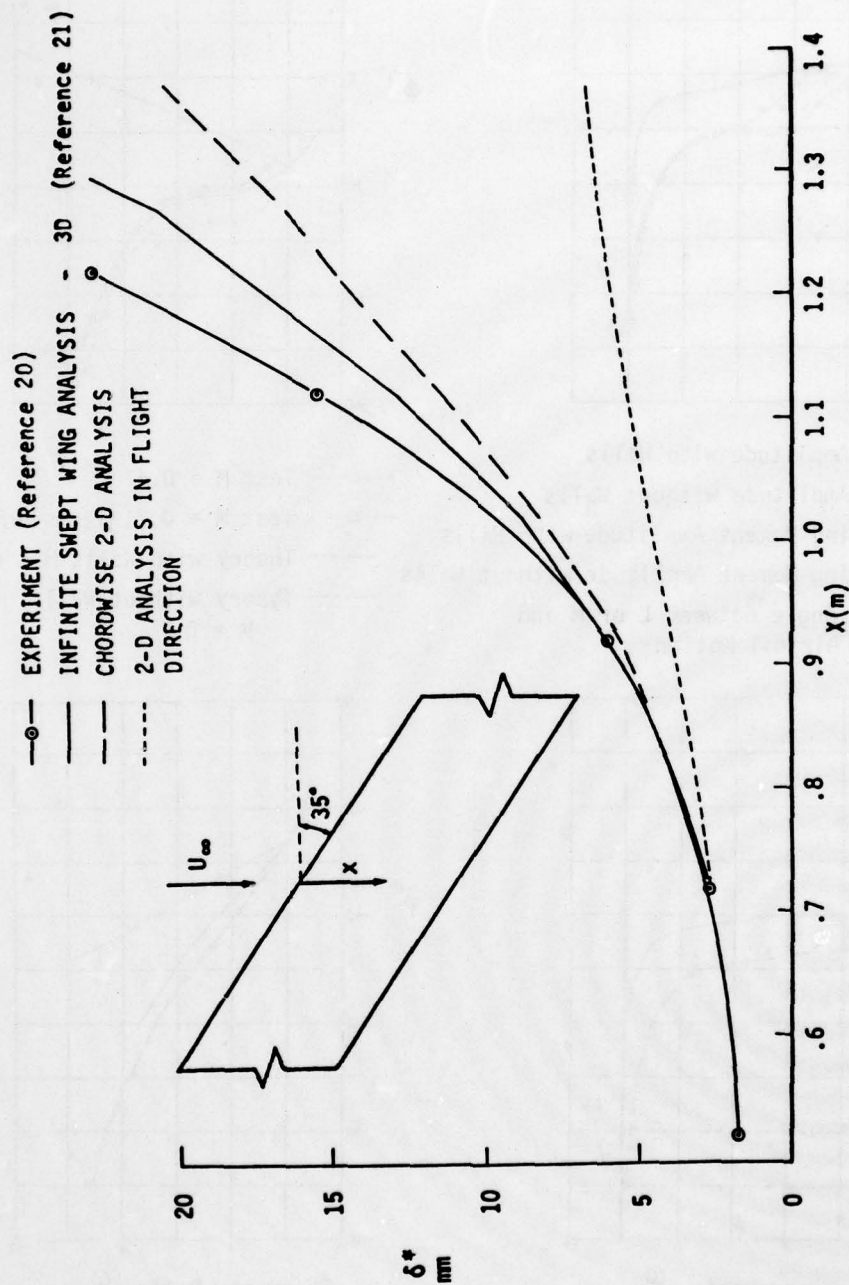
Figure 8. Quasi-Planar Approximation of the Boundary Layer (McLean, Reference 21)
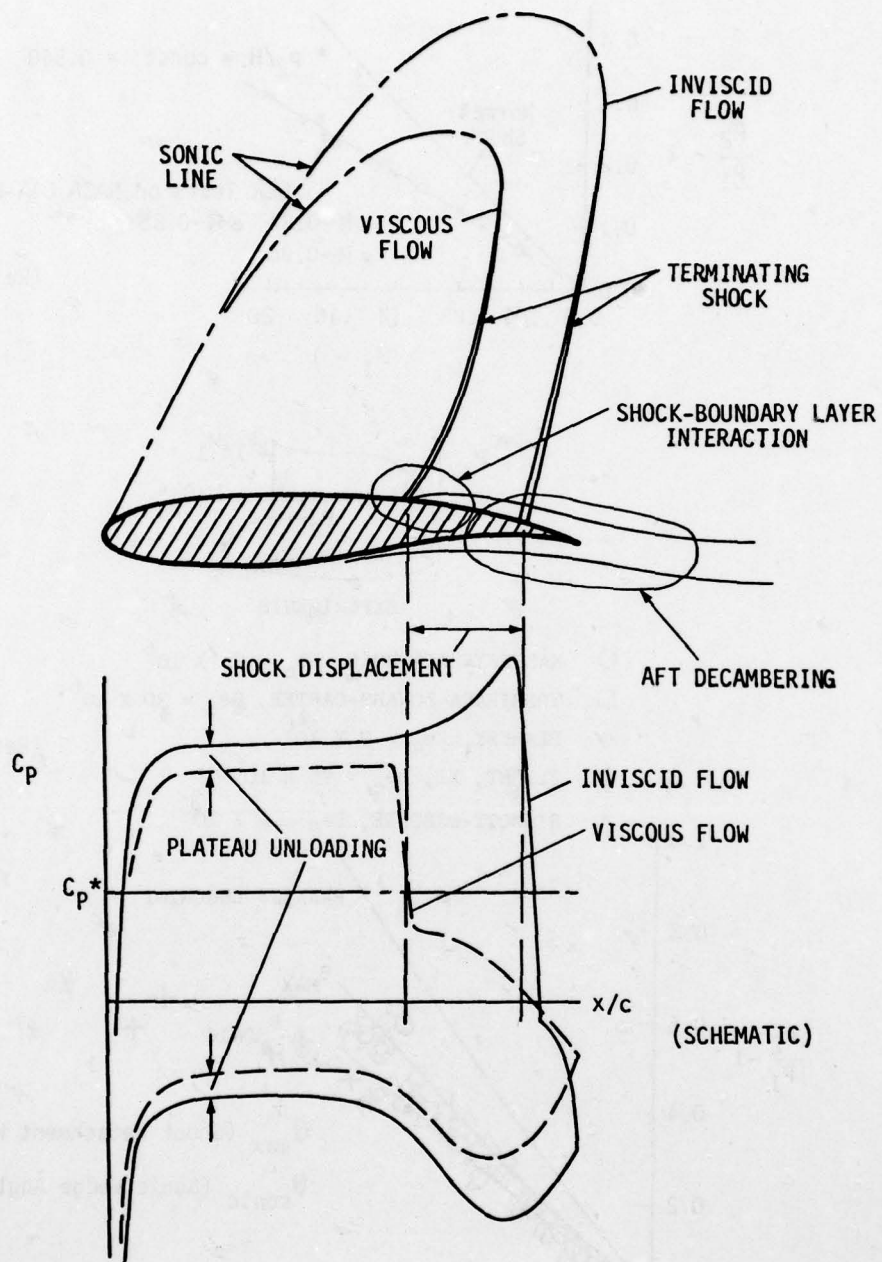
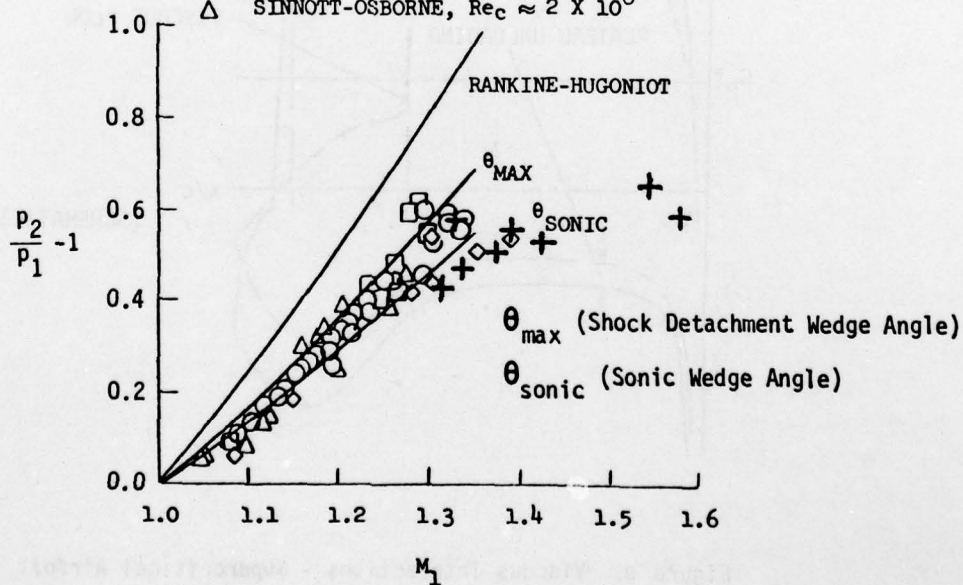Figure 9. Viscous Interactions - Supercritical Airfoil
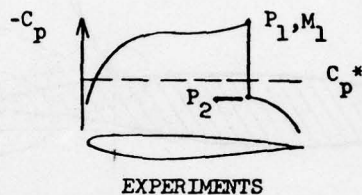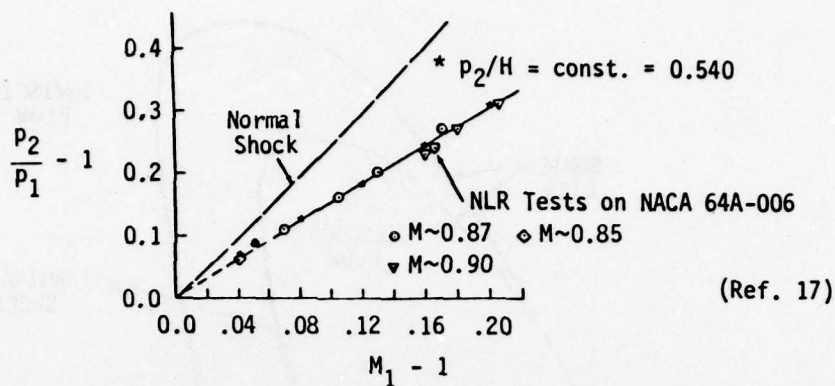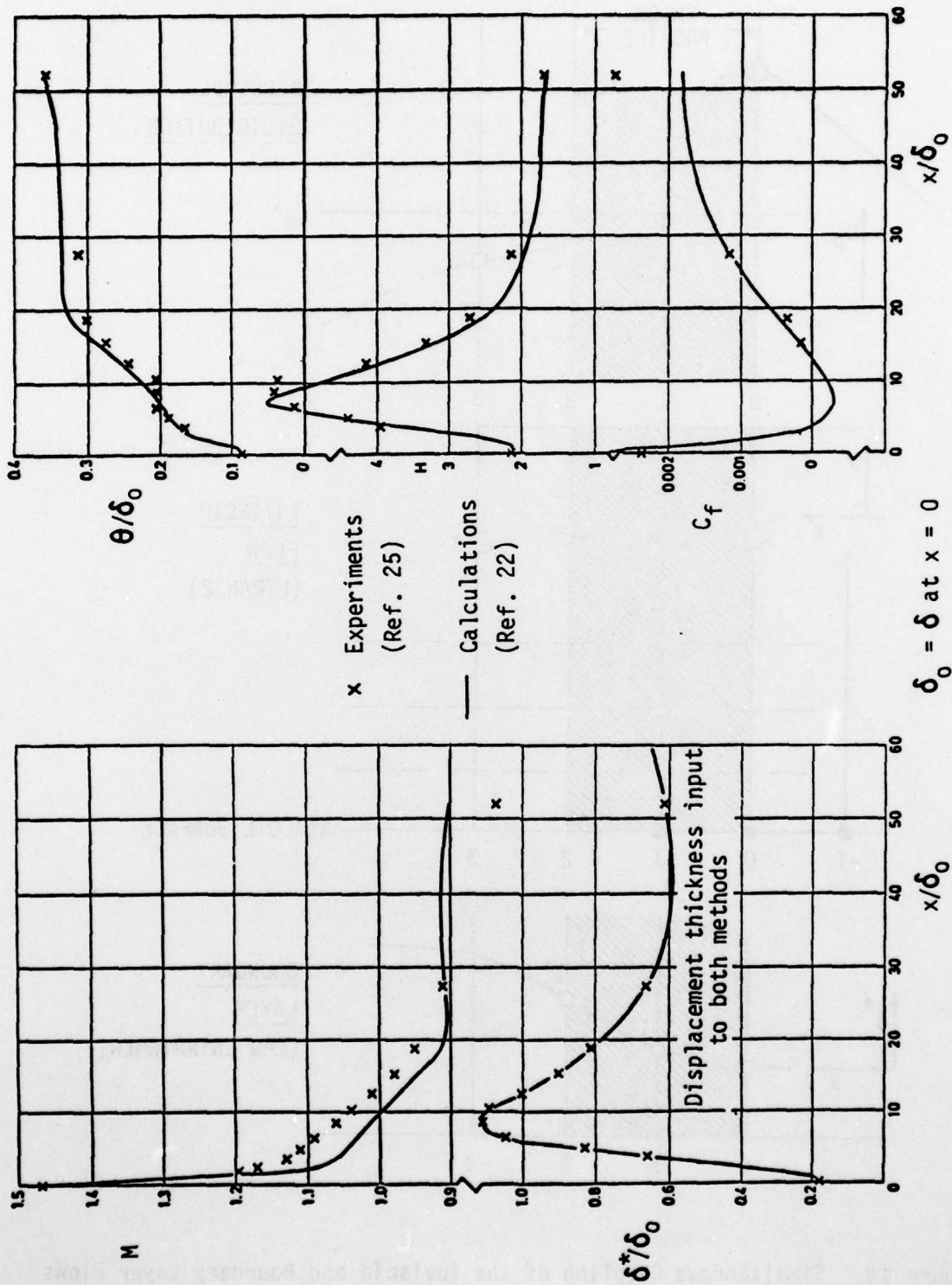
Figure 10. Measured Post-Shock Pressures

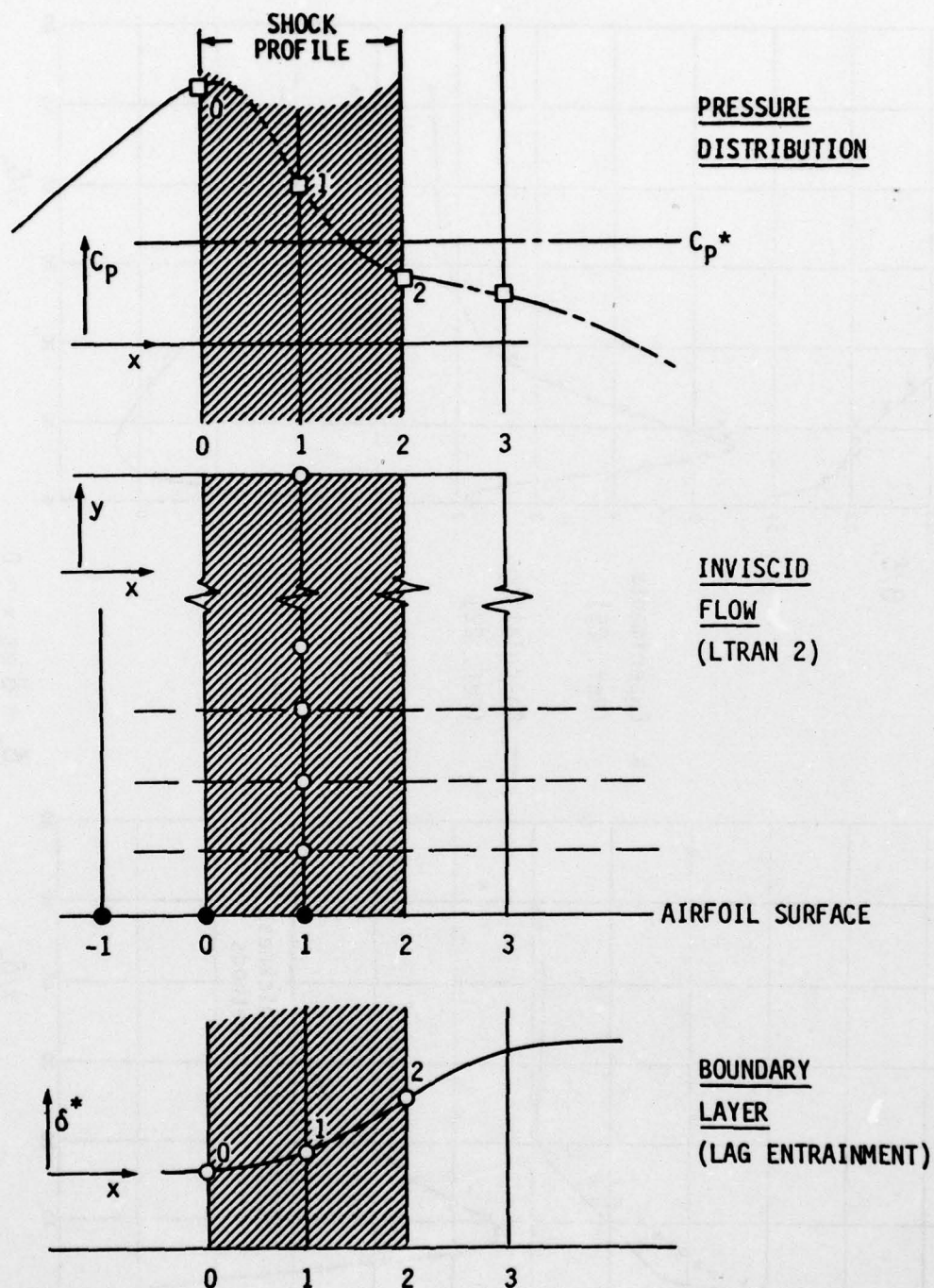Figure 11. Green's Lag Entrainment Method in the Case of Seddon's Flow

Figure 12. Simultaneous Coupling of the Inviscid and Boundary Layer Flows

78